Simulation and Sensitivity Analysis of Spiral Wound Reverse Osmosis Process for the Removal of Dimethylphenol from Wastewater Using 2-D Dynamic Model

Mudhar A. Al-Obaidi [1, 2], Chakib Kara-Zaïtri [1] and Iqbal M. Mujtaba [1, *]

[1] **Chemical Engineering, School of Engineering, Faculty of Engineering and Informatics. University of Bradford. Bradford, West Yorkshire BD7 1DP, UK**
[2] **Middle Technical University, Iraq – Baghdad**
***Corresponding author, Tel.: +44 (0) 1274 233645**
E-mail address: I.M.Mujtaba@bradford.ac.uk

Abstract

Reverse Osmosis (RO) processes are readily used for removing pollutants, such as dimethylphenol from wastewater. A number of operating parameters must be controlled within the process constraints to achieve an efficient removal of such pollutants. Understanding the process dynamics is absolutely essential and is a pre-step for designing any effective controllers for any process. In this work, a detailed distributed two-dimensional dynamic (x and y dimensions and time) model for a spiral-wound RO process is developed extending the 2-D steady state model of the authors published earlier. The model is used to capture the dynamics of the RO process for the removal of dimethylphenol from wastewater. The performance of the 2-D model is compared with that obtained using 1-D dynamic model before the model is being used to investigate the performance of the RO process for a range of operating conditions.

***Keywords*:** Reverse Osmosis; Spiral-wound Module; Simulation; Sensitivity Analysis; Dimethylphenol Removal; Wastewater Treatment.

1. Introduction

Pressure-driven membrane technology has been widely used in a variety of applications ranging from seawater desalination to wastewater treatment because of its versatility including: no further chemical treatment requirements, low- energy demand and low capital and operating costs, compared to other thermal techniques such as MSF. It is not surprising therefore that such technologies as RO have been used ubiquitously in both seawater and wastewater treatment, and have yielded effective solutions for improved water quality (Fritzmann *et al.*, 2007; Singh *et al.*, 2013; Goh *et al.*, 2016).

The spiral-wound module is the most commonly used model in reverse osmosis as, it can readily be applied in a variety of different applications. Having said this, there remains the

challenge of having a reliable design for high process performance of the process and the critical need for an accurate mathematical modelling methodology. This usually consists of a set of ordinary algebraic and differential equations, which are used to predict the process behaviour and thus facilitate the implementation of an effective optimisation process for minimising technical risks and costs. Several mathematical models can be found in the literature for the RO membrane module transport phenomena. However, the majority of these models rely on approximate calculations based on average conditions of the membrane sides without considering the variation of operating parameters along the membrane dimensions. Furthermore, few models have been developed to characterise the transport phenomena in one and two dimensions of the spiral-wound RO process considering the removal of high-toxic compounds (such as dimethylphenol) from wastewater. This is compared to the several attempts of developing distributed models in one and two dimensions for seawater and brackish water desalination process (Avlonitis *et al.*, 1991, 1993, 2007; Boudinar *et al.*, 1992; Geraldes *et al.*, 2005; Senthilmurugan *et al.*, 2005; Li, 2012). It is important to note that the two-dimensional modelling has the advantage of providing a facility for predicting the process performance more accurately than the one-dimensional modelling. This is because the pattern of feed flow rate along the tangential direction for both the retentate and permeate sides are taken into consideration. It can also be argued that the dynamic modelling can yield other advantages compared to steady state modelling. This includes the time parameter, which allows the modelling of the behaviour of the process against the operational time. It is therefore highly advantages to have a dynamical model capable of yielding a more efficient process control strategy and yet maintain the separation cost at an acceptable level. Examples of previous work in this aspect are described in the next section.

Sagne *et al.* (2009) suggested a 1D dynamic model from the solution-diffusion model but neglected the impact of concentration polarisation on the dilute aqueous solution rejection of five organic compounds (Acetic acid, Butyric acid, Furfural, 2-Phenylethanol and 2,3-Butanediol) from brackish water serviced in the fermentation industries. A comprehensive lumped-model based on the solution-diffusion principle has been developed by Oh *et al.* (2009) for the simulation and optimisation of the RO process regardless of the type of the membrane used. Based on the three-parameter model of Spiegler and Kedem (1966), Mane *et al.* (2009) developed a model for a turbulent flow by considering the two dimensions (x and y) for the feed flow rate and stimulated the rejection of boron by the RO process. A nonlinear ordinary differential equations dynamic model-based control system on an experimental spiral-wound RO membrane seawater desalination system is developed by Bartman *et al.*

(2009) and (2010). The model developed is used to design a nonlinear control system, using geometric control techniques and to design and implementation of an optimization-based control system respectively. For an industrial scale RO desalination process, Chen-Jen Lee (2010) studied the dynamic characteristics and process operation by developing a mathematical one-dimensional dynamic model. This work has combined the model of Oh *et al.* (2009) with that of Marriot *et al.* (2003) and considered the impact of solvent flux on the retentate concentration.

Except a handful of models described below, all the developed dynamic models for spiral-wound RO process described above, have been validated against experimental data derived for sea and brackish water.

A lumped-model has been developed by Ahmad *et al.* (2007) for unsteady state simulation and validated against experimental data of the pre-treated palm oil mill effluent as a feed using a pilot-plant scale RO system. A one-dimensional steady state model is developed by Sundaramoorthy *et al.* (2011a,b), which is based on the principles of the solution-diffusion model and assumed constant pressure and concentration at the permeate channel. The model prediction is compared with experimental data of chlorophenol and dimethylphenol solutes separately. Fujioka *et al.* (2014) developed a one-dimensional steady state model based on the irreversible thermodynamic model and considered a variety of operating parameters by assuming zero permeate pressure. This model was confirmed against experimental data of N-nitrosamine rejection. More recently, Al-Obaidi *et al.* (2016) developed a one-dimensional dynamic model to predict the performance of an individual spiral-wound RO membrane to remove chlorophenol from wastewater.

To the best of authors' knowledge there is no study in terms of development of two-dimensional (2-D) dynamic model (X and Y dimensions and time) or its use for spiral wound RO process-based wastewater treatment except the 2-D steady state simulation studies presented by Al-Obaidi *et al.* (2017).

In this work, we extend the recently developed 2-D steady state model of Al-Obaidi *et al.* (2017) to a 2-D dynamic model and use the model to study the dynamic response of the RO process while removing dimethylphenol from wastewater. To justify the use of a 2-D dynamic model we compare the performance of the RO process with those obtained by 1-D model under steady state condition. Finally, we use the 2-D model to study the dynamic behavior and the sensitivity of the unit performance to a variety of operating parameters.

2. Dynamic modelling platform and the 2-D model

Fig. 1 shows the spiral-wound RO two-dimensional dynamic modelling platform, which consists of the required model equations and mass transfer coefficient model in addition to the physical property models.

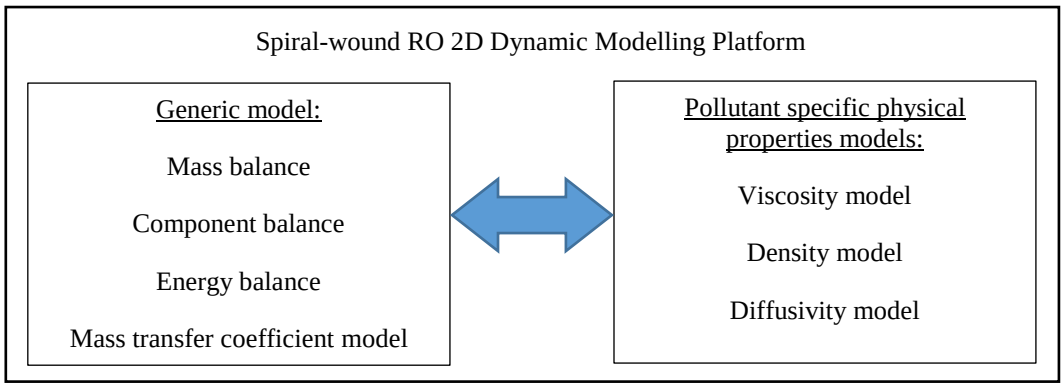

Fig. 1. The modelling platform of RO

Fig. 2 shows the spiral-wound module, which contains the main two parts, i.e. the feed and permeate sides. The detailed sizes of the membrane are the length L and width W, and the feed t_f and permeate t_p spacers channels. Therefore, the effective membrane area can be given as ($A_m = L\,W$). Also, x denotes the axial coordinate along the membrane length, and y denotes the tangential coordinate in the spiral direction starting from the sealed end of the leaf to the end of membrane width. Taking into the consideration of two-dimensional distributed modelling requirements, the membrane area was split into 36 sub-sections of equal areas ($\Delta x, \Delta y$) using the method of discretisation used by gPROMS suite (Process System Enterprise Ltd., 2001). Therefore, the variety of all operating parameters along the two dimensions will be characterised at each point of the membrane length and width. Also, each sub-section area is attained by, ($A_{sub-section} = \Delta x\,\Delta y$), where $\Delta x = \frac{L}{6}$ and $\Delta y = \frac{W}{6}$.

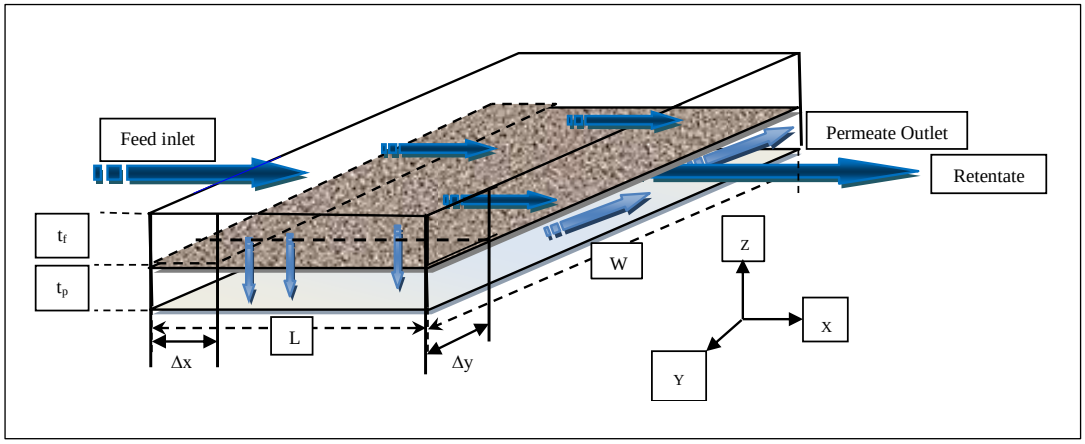

Fig. 2. Diagram of the spiral-wound module (Adopted from Al-Obaidi *et al*., 2017)

The final 2-D dynamic model together with the physical properties calculations of the dimethylphenol solutions can be shown in Table A.1 in Appendix A with the degree of freedom analysis (Table A.2 and A.3 in Appendix A). Note, the discretisation method described above converted the partial differential equations (PDEs) into ordinary differential equations (ODEs) which allow calculating the values of any variables at the discrete point (x, y) but at any time. There are many mathematical techniques in converting PDEs into ODEs. In this work we used the built-in techniques in gPROMs software (Process Systems Enterprise Ltd., 2001). The main assumptions of the model are: (a) the membrane is made up of a non-porous flat sheet and negligible leaf curvature (b) the pressure drop is proportional to the feed and permeate flow rate in the case of laminar flow conditions and the friction parameter is used to characterize the pressure drop (Darcy's law) (c) the friction factor of feed and permeate channels is assumed constant due to laminar flow (d) negligible impact of feed spacer on the fluid patterns at the feed channel (e) isothermal process. Note, the wound membrane is basically treated as unwound which has a similar configuration of the plate-and-frame module. This assumption was made by several researchers such as Senthilmurugan *et al.* (2005) and Sundaramoorthy *et al.* (2011a). This assumption is used to simplify the complex configuration of a spiral wound RO module. Also note, Gu *et al.* (2017) developed a successful one-dimensional model despite neglecting the presence of feed spacer and this model was validated against experimental data of seawater desalination (although not for wastewater treatment).

The validation of our 2-D dynamic model was carried out against experimental data of Srinivasan *et al.* (2011) for the removal of dimethylphenol from wastewater by Al-Obaidi *et al.* (2017) but under steady state condition.

The procedure for the solution of model equations is by dividing the whole unit of the spiral-wound module to a number of equal individual sub-sections in two dimensions. Also, a guess

for the initial value of the permeate pressure (close to 1 atm) at the entrance of the permeate channel will be considered to ensure 1 atm at the perforated pipe. Then by using a numerical solution (approximate solution) in the gPROMS software suite, water, and solute fluxes with the values of retentate and permeate concentrations, pressures, temperatures, flow rates and wall concentration will be calculated for each sub-section. gPROMS is one of the best industrial standard modelling platform used for many years for solving distributed models with integral, partial, and ordinary differential and algebraic equations where properties vary in one or more spatial dimensions as well as time. The model equations shown in Table A.1 in Appendix A is solved using the numerical method of Orthogonal Collocation on Finite Elements (OCFEM) of order 2. This contains discretisation of the distributed equations with respect to all spatial domains (X and Y) and elucidates the numerical solutions of the variables. One of the main specifications that needs to be determined before solving the model equation is the number of discretization intervals, which has a significant impact on the solution trajectory. It is noticed that selecting a small number of intervals (4) or fine grid (high number of intervals) such as (64) will result in an accurate solution and a steep gradient problem of inefficient solution respectively. However, we found that 36 sub-sections selection provides closer solution with very good computational efficiency. Figs. A1 and A2 in Appendix A show the profile of feed concentration and permeate concentration respectively along the two dimensions (*x* and *y*) in the feed and permeate channels using the 36 sub-sections at different operating time. Also, Figs. A3 – A.6 in Appendix A show the profile of feed pressure, feed flow rate, feed concentration, and permeate concentration respectively along the two dimensions (*x* and *y*) in the feed and permeate channels using the 4 and 36 sub-sections at t = 2000 sec. Moreover, Table A.4 in Appendix A shows the grid sensitivity analysis. This in turn confirms variation of operating parameters against the operating time and the accuracy of selecting 36 sub-sections to predict the operating parameters. Moreover, it is noticed that increasing the order of OCFEM higher than 2 causes inaccurate solutions.

3. Experimental setup and parameter estimation

Srinivasan *et al.* (2011) used a spiral-wound module (Ion Exchange, India Ltd.) in a laboratory scale RO system to remove dimethylphenol at different concentrations from its aqueous solutions. Table 1 shows the characteristics of the module used. The solute concentrations of dimethylphenol varies from 0.819×10^{-3} to 6.548×10^{-3} kmol/m³. The feed

flow rates of 2.166×10^{-4}, 2.33×10^{-4} and 2.583×10^{-4} m^3/s and feed pressures varying between 5.83 and 13.58 atm are used respectively.

The model includes some unknown parameters such as the solvent and solute transport coefficients (A_w, B_s) and the feed channel friction parameter *b*. These were evaluated by Al-Obaidi *et al.*, 2017 using a graphical linear method proposed by Sundaramoorthy *et al.* (2011a). The results of the parameter estimation methodology are given in Table 1, which showed a minor difference than the values estimated by Srinivasan et al. (2011).

Table 1. Membrane specifications

Maker and configuration	Ion Exchange, India Ltd., TFC Polyamide, spiral wound
Membrane width (W)	8.4 m
Membrane length (L)	0.934 m
Active surface area (A)	7.9 m^2
Module diameter	3.25 inches
Permeate channel thickness (t_p)	0.5 mm
Number of turns	30
Feed channel thickness (t_f)	0.8 mm
b	9400.9 $\left(\frac{atm\ s}{m^4}\right)$
A_w and B_s (Dimethylphenol)	9.42009×10^{-7} $\left(\frac{m}{atm\ s}\right)$ and 2.22577×10^{-8} $\left(\frac{m}{s}\right)$

4. Comparison of performance using 1-D model

Al-Obaidi *et al.* (2016) developed 1-D dynamic and steady state model for the removal of chlorophenol from wastewater. In this work we use their model for the removal of dimethylphenol from the wastewater (by incorporating appropriate thermophysical properties of the contaminant). The prediction of several key parameters ($Rej_{(av)}$ and $Rec_{(Total)}$) of the process is outlined in Table 2 together with the prediction of the same parameters obtained using the 2-D model of this work (under steady state condition).

As can be seen from Table 2, the accuracy of prediction using 2-D model has significantly improved compared to experimental results thus justifying further investigation of the process using 2-D model.

Table 2. Comparison of 1-D and 2-D models predictions against experimental data of Srinivasan *et al.* (2011) for the removal of dimethylphenol from wastewater

Exp. Nu.	$C_{b(inlet)}$ (kmol/m³) x10^3	$P_{b(inlet)}$ (atm)	$F_{b(inlet)}$ (m³/s) x10^4	Tb (°C)	Parameter	Exp. value (Srinivasan *et al.*, 2011)	1D Model	error%	2D Model	error%
1	6.548	13.58	2.583	31.5	$Rej_{(av)}$	97.3	96.5373	0.783	98.0197	-0.739
					$C_{b(outlet)}$	0.00850	0.0088	-3.853	0.00878	-3.326
					$Rec_{(Total)}$	22.1447	27.0909	-22.33	25.6416	-15.790
					$F_{b(outlet)}$	2.01x10^{-4}	1.9x10^{-4}	5.700	1.93x10^{-4}	3.787
2	6.548	11.64	2.583	31.5	$Rej_{(av)}$	96.9	95.9413	0.989	97.7175	-0.843
					$C_{b(outlet)}$	0.00800	0.0083	-3.682	0.00826	-3.202
					$Rec_{(Total)}$	19.0863	22.1123	-15.854	20.8074	-9.017
					$F_{b(outlet)}$	2.09x10^{-4}	2.02x10^{-4}	3.311	2.05x10^{-4}	1.810
3	6.548	9.71	2.583	31.5	$Rej_{(av)}$	96.3	95.0446	1.303	97.2688	-1.006
					$C_{b(outlet)}$	0.00782	0.0078	-0.080	0.00780	0.311
					$Rec_{(Total)}$	15.9891	17.1569	-7.303	15.9702	0.118
					$F_{b(outlet)}$	2.17x10^{-4}	2.14x10^{-4}	1.178	2.17x10^{-4}	0.037
4	6.548	13.58	2.33	31.5	$Rej_{(av)}$	97.3	96.5654	0.754	98.0130	-0.732
					$C_{b(outlet)}$	0.00867	0.0091	-5.821	0.00913	-5.326
					$Rec_{(Total)}$	25.5793	30.1017	-17.679	28.5398	-11.573
					$F_{b(outlet)}$	1.73x10^{-4}	1.64x10^{-4}	5.273	1.68x10^{-4}	3.058
5	6.548	11.64	2.33	31.5	$Rej_{(av)}$	96.9	95.9834	0.945	97.7124	-0.838
					$C_{b(outlet)}$	0.00818	0.0085	-4.606	0.00851	-4.118
					$Rec_{(Total)}$	22.1030	24.6555	-11.548	23.2545	-5.209
					$F_{b(outlet)}$	1.82x10^{-4}	1.77x10^{-4}	2.720	1.80x10^{-4}	0.981
6	6.548	9.71	2.33	31.5	$Rej_{(av)}$	96.2	95.1263	1.116	97.2753	-1.117
					$C_{b(outlet)}$	0.00781	0.0080	-2.597	0.00798	-2.180
					$Rec_{(Total)}$	18.3690	19.2215	-4.640	17.9640	2.204
					$F_{b(outlet)}$	1.90x10^{-4}	1.89x10^{-4}	0.730	1.91x10^{-4}	-0.580

5. Dynamic simulation using 2-D model

One characteristic of any industrial process is the possibility of sudden and sustained step change in input parameters, which causes a corresponding change in the process performance. This section deals with the using of the dynamic model to reproduce the process and analyse the sensitivity of the RO performance process under various operating parameters. The dynamic model is simulated by changing several parameters (one at a time). Most importantly, the selected variation of the operating parameters including the feed pressure, concentration, flow rate and temperature are selected as the main operating parameters in the experimental work of Srinivasan *et al.* (2011). The degree of freedom (*DoF*) calculation is provided in Appendix A and the input data is shown in Table A.3.

The effects of processing parameters on the RO module performance are labelled in the following sections.

5.1. The inlet feed pressure

Figs. 3 to 7 show the impact of a step change for the operating pressures on the solute rejection, average permeate concentration, average retentate concentration, total water recovery and average retentate flow rate for various inlet feed concentrations at fixed temperature and inlet feed flow rate.

For the first 600 s, the feed pressure was 9.71 atm and after then the operating pressure is increased by 40 % to 13.58 atm. Note that, Figs. 3, 6 and 7 are intentionally drawn with different time axes than in Figs. 4 and 5 so as to show the impact of the step change in a clearer way on the specific parameters. The reason for the difference is that the steady state condition specifically achieved is in fact faster for the parameters of Figs. 3, 6 and 7. Note that the selected operating pressure is within the experimental data of Srinivasan *et al.* (2011). This is also quite low to what is usually used for seawater desalination RO process, to overcome the high osmotic pressure (high salt concentrations of seawater).

It is not difficult to see that increasing the inlet feed pressure actually raises the average retentate concentration (Fig. 3), decreases the average permeate concentration (Fig. 4), increases the solute rejection (Fig. 5), increases the total water recovery (Fig. 6) and decreases the retentate flow rate (Fig. 7) for all the tested inlet feed concentrations. This phenomenon could be described as an increase of the water flux traveling through the membrane because of a raise of the inlet feed pressure. Since the domino effect, the increase of the pressure results to a higher permeate flux due to a reduction of concentration polarisation impact, which in turn causes a rise of the retentate concentration and a reduction

of the permeate concentration due to a high level of dilution. Eq. (1) in Table A.1 in Appendix A shows that the water flux $J_{w(x,y)}$ increases due to a growth in the feed pressure, which raises the trans-membrane pressure $\Delta P_{b(x,y)}$ above the osmotic pressure term. Consequently, the solute rejection is improved due to an improvement of the water flux. Also, the quantity of permeated water increases and causes higher levels of water recovery. For this reason, the retentate flow rate decreases as a result to an increase in the operating pressure.

Figs. 3 and 4 show that the impact of a step change in the operating pressure is slightly more visible at higher concentration solution than the lower ones. In other words, the retentate and permeate concentration of the high concentration solutions are more likely to be affected by the step change of operating pressure than lower concentration solutions. This is mainly due to lifting the quantity of water flux as a response to operating pressure increase. However, it is expected that increasing the water flux at the high concentration solutions would have a significant influence on the concentration polarisation and solute concentration both in the feed and permeate channels compared to other solutions with lower solute concentration. Consequently, this will lead to a higher overshoot in the retentate concentration (Fig. 3) and a lower overshoot in the average permeate concentration (shown as in Fig. 4) in response to an increase in the inlet feed pressure. Interestingly, Fig. 4 shows that the average permeate concentration has shown a unique underdamped response, where it exhibits no overshoots before getting to steady state condition. This is quite different when compared to other operating parameters studied where it shows slight and sharp overshoots. This is quite reasonable due to recognizing that the step change of operating pressure is directly subjected to the feed channel, where the feed flow rate and retentate concentrations are directly affected compared to the permeate concentration at the permeate channel. Therefore, there is no sharp response with overshoot at the permeate concentration. Fig. 5 shows the influence of the solute rejection progresses with an increase of the inlet feed concentration and this was attributed to a rise of the membrane solute isolation strength (Al-Obaidi and Mujtaba, 2016). Another reason is that rising the inlet feed concentration causes an increase in the osmotic pressure and the permeate concentration. However, the increase of permeate concentration is insignificant with the increase of bulk concentration in the feed channel, which itself results in an increase in the solute rejection commensurate with Eq. (15) in Table A.1 in Appendix A. A similar trend of results was confirmed for all the three types of membranes tested by Gómez *et al.* (2009). However, the solute rejection is mainly dependent on both the retentate

concentration and permeate concentration, which relatively showed a response with overshoot (Fig. 5).

Fig. 6 shows that the total water recovery decreases with an increase of the inlet feed concentration. It can be ascribed as a rise of the osmotic pressure which declines the motivation of water flux and hence diminishes the quantity of permeated water in the permeate channel. For the same reason, the retentate flow rate decreases because of an increase of the operating concentration (Fig. 7).

Fig. 4 shows that the setting time for an average permeate concentration at the permeate channel for the higher inlet feed concentration is a bit longer compared with the lower feed concentration. This is mainly because a higher solute concentration medium requires more time to settle than the lower ones (for a given volume) and vice versa. Also, Fig. 5 readily confirms a number of key observations:

- that the steady state solute rejection was reached between 200 and 250 s for the tested inlet feed concentrations, albeit with a little bit of a difference.
- that the solute rejection transient response of the lower feed concentration to feed pressure is irrelevant compare with a higher feed concentration solution. This is owing to a higher water flux occurring when using a lower feed concentration medium in comparison with a higher feed concentration medium with the impact of concentration polarisation.
- that the solute rejection begins at $t = 0$ at its maximum because there is no concentration polarisation in the start time. Having said this, the solute rejection is gradually retarded as the solute starts to be retained along the membrane wall until settled at a constant value.

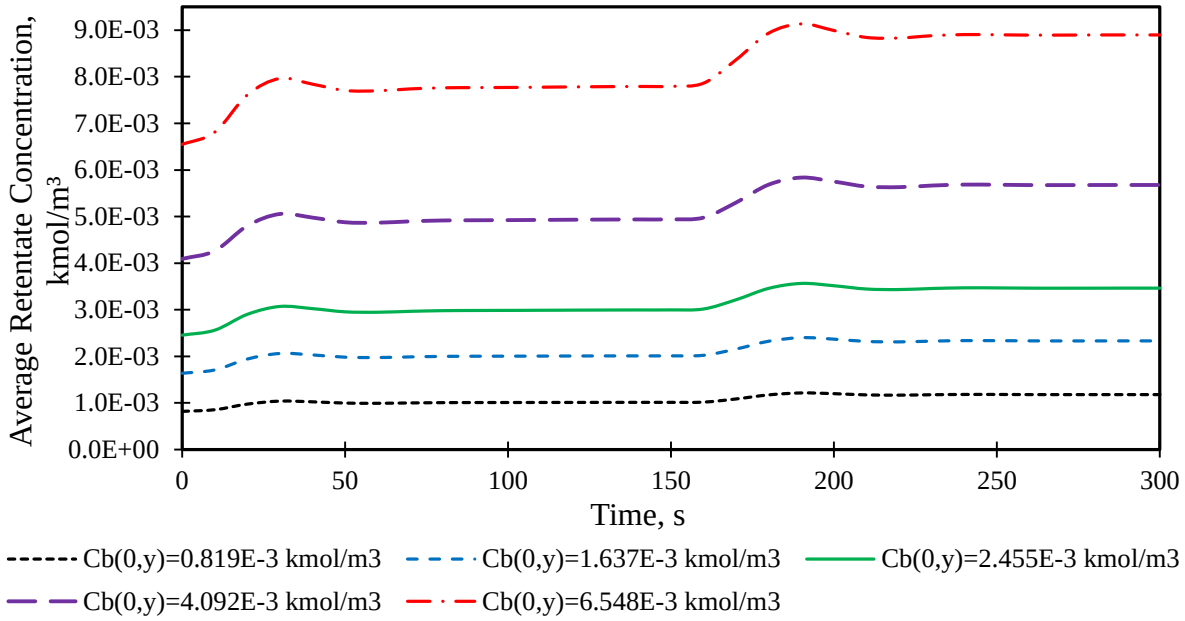

Fig. 3. The result of the step change of operating pressure on retentate concentration for several operating concentrations at operating conditions of $2.583x10^{-4}$ m³/s, 9.71 atm and 31.5 °C

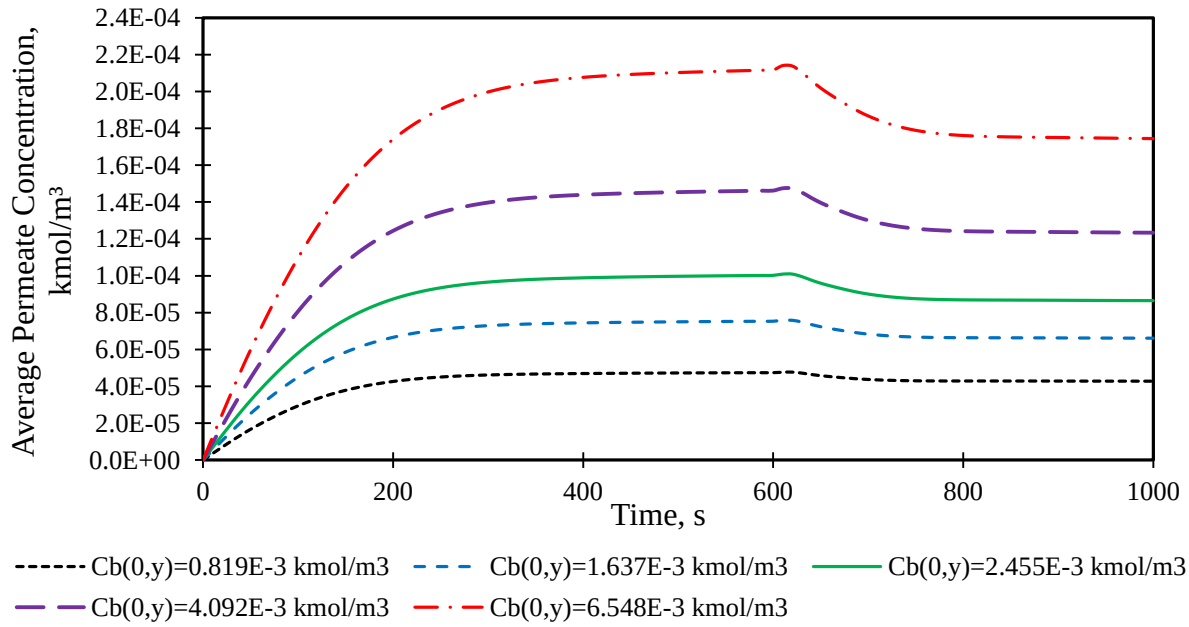

Fig. 4. The result of the step change of operating pressure on mean permeate concentration for several operating concentrations at operating conditions of $2.583x10^{-4}$ m³/s, 9.71 atm and 31.5 °C

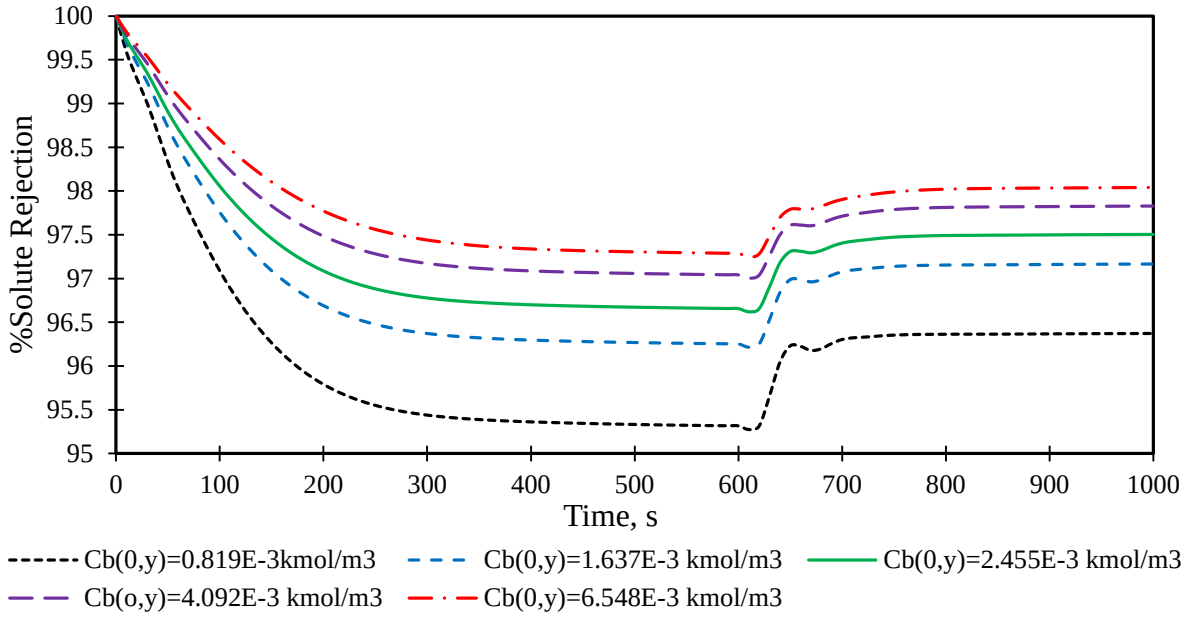

Fig. 5. The result of the step change of operating pressure on solute rejection for several operating concentrations at operating conditions of $2.583x10^{-4}$ m³/s, 9.71 atm and 31.5 °C

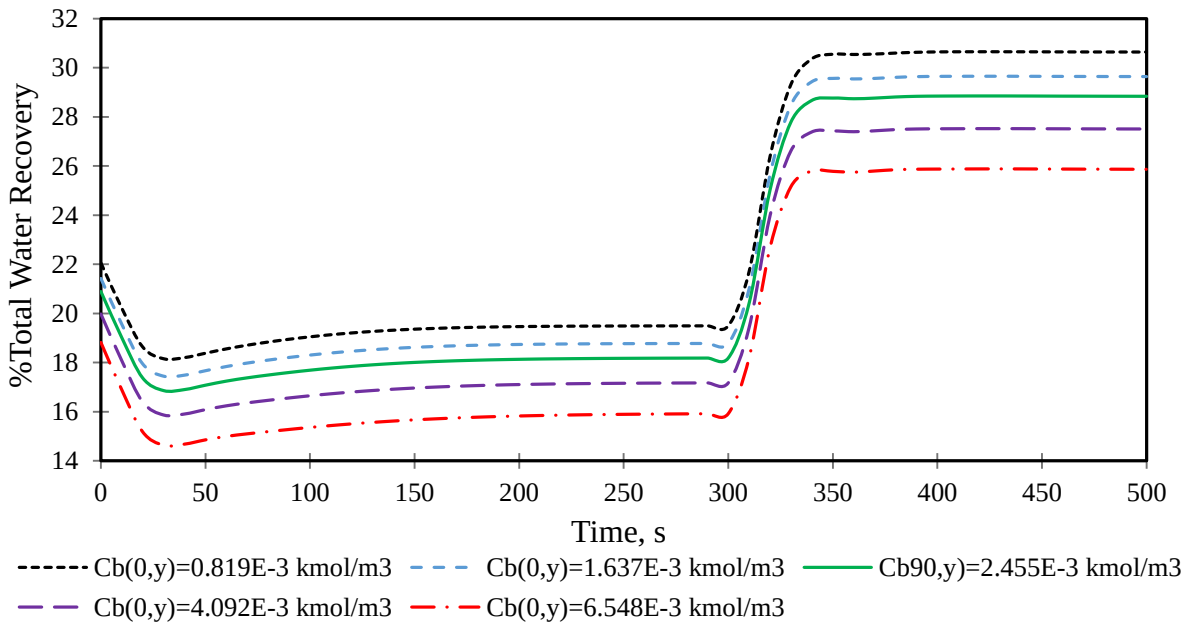

Fig. 6. The result of the step change of operating pressure on total water recovery for several operating concentrations at operating conditions of $2.583x10^{-4}$ m³/s, 9.71 atm and 31.5 °C

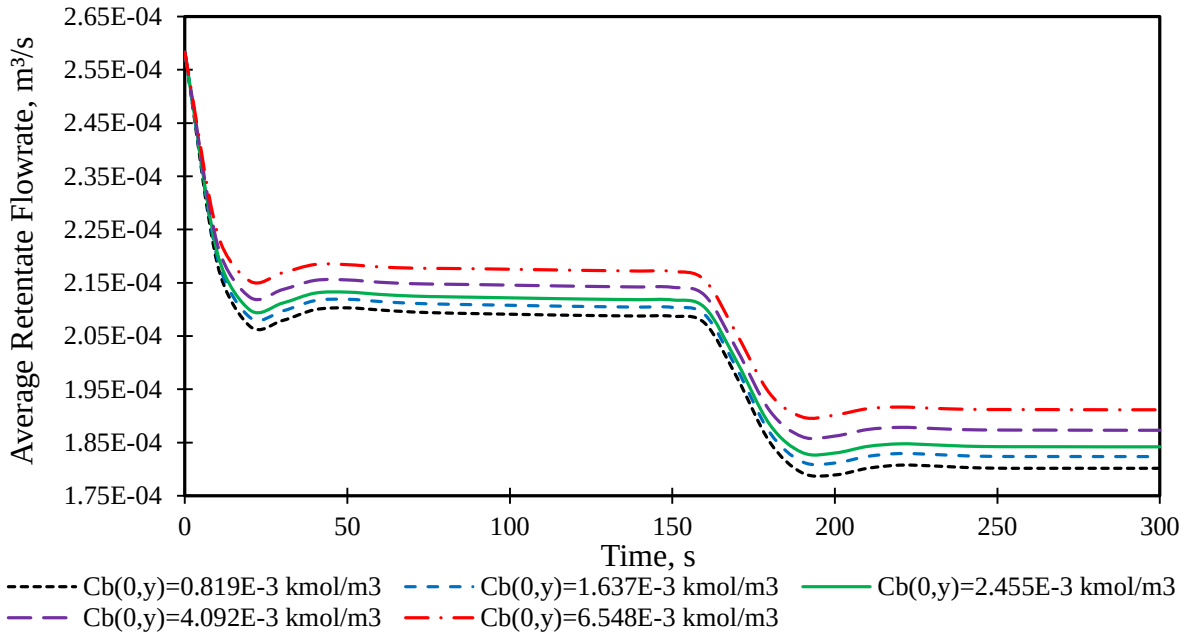

Fig. 7. The result of the step change of operating pressure on retentate flow rate for several operating concentrations at operating conditions of $2.583x10^{-4}$ m³/s, 9.71 atm and 31.5 °C

Moreover, it is possible that any industrial process may be subjected to a ramp change of operating conditions, which is basically carried out in a gradual upward or downward change for a period of time with constant slop. Fig. 8 shows the impact of a ramp change in the operating pressure on the solute rejection at fixed operating concentration, flow rate and temperature. For the first 600 s, the feed pressure was 10 atm and then it is increased to 12, 14 and 16 atm at 600, 900 and 1200 s respectively.

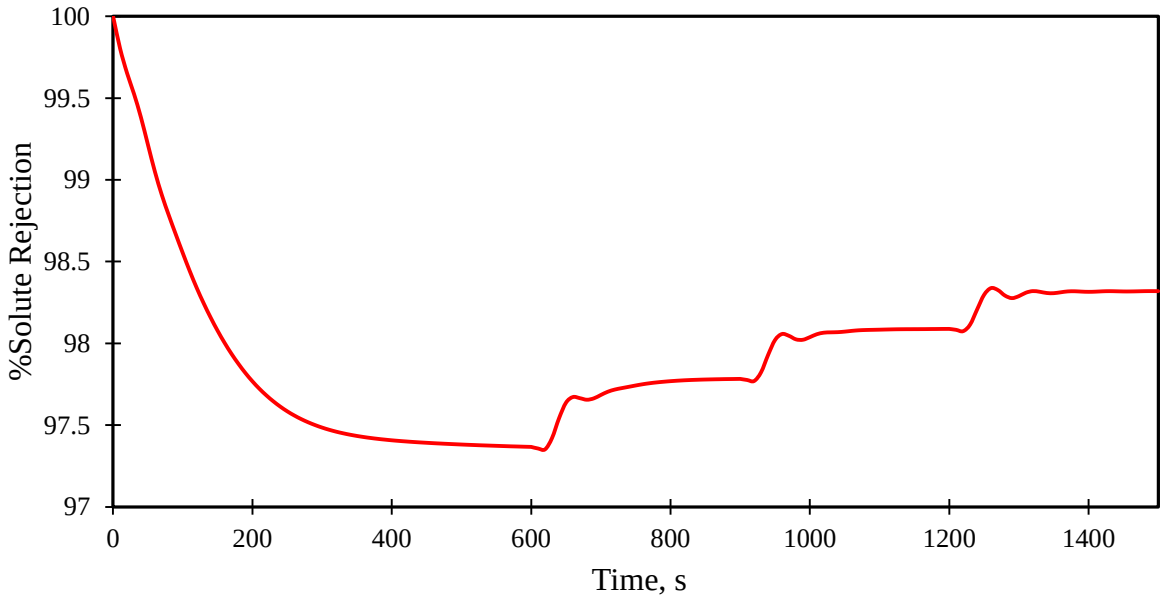

Fig. 8. The result of the ramp change of operating pressure on solute rejection for operating conditions of $6.548x10^{-3}$ kmol/m³, $2.166x10^{-4}$ m³/s, 10 atm and 31.5 °C

As it is expected, the progress of operating pressure at fixed other operating parameters causes an increase in the solute rejection. Also, it can be noticed that the ramp change of 2 atm increase has relatively different settling time, where the process can quickly be settled at higher operating pressures. Increasing permeated water is observed as a response to increasing operating pressure that reduces the settling time of permeate concentration (Fig. 9).

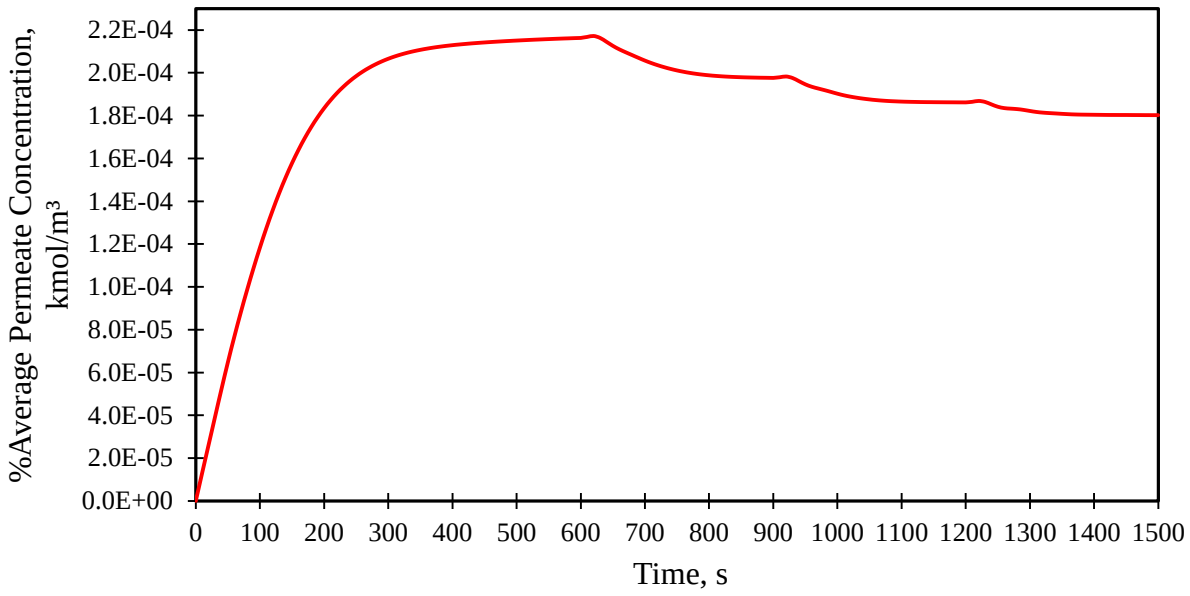

Fig. 9. The result of the ramp change of operating pressure on average permeate concentration for operating conditions of 6.548×10^{-3} kmol/m³, 2.166×10^{-4} m³/s, 10 atm and 31.5 °C

5.2 The inlet feed flow rate

Figures 10 to 12 show the relation of the step change of the operating feed flow rate and the average retentate concentration, rejection and average permeate concentration for several operating pressures under constant operating concentration and temperature. For the first 1000 s the operating feed flow rate is 2.33×10^{-4} m³/s while at t = 1000 s, the operating feed flow rate is increased to 2.583×10^{-4} m³/s. Note that, Fig. 10 is intentionally drawn with different time axes than in Figs. 11 and 12 so as to show the impact of the step change in a clearer way on the specific parameters.

It can be seen that the system has settled within 200 – 250 s during the step change of the inlet feed flow rate. Interestingly, this is quite similar to the case of a step change of inlet feed pressure.

Increasing the inlet feed flow rate causes a reduction in the concentration polarisation along the membrane, which leads to the increase of the mass transfer coefficient and the reduce of the solute concentration at the feed channel and average permeate concentration at the permeate channel.

Fig. 10 shows that the retentate concentration endures a quick increase tracked by an instant high-pitched reduction before reaching a new fixed state after about 150 s as a reply to a step change in the inlet feed flow rate. The retentate concentration seems to decrease more when using higher pressure conditions. Moreover, it is not difficult to see that the transient response of the average permeate concentration (Fig. 11) is much slower than the response of the retentate concentration for the same step change in the operating feed flow rate (Fig. 10). Fig. 10 shows that the transient effects of the retentate concentration at higher pressure conditions on step change in the feed flow rate is larger than the lower feed pressure conditions. In other words, a higher degree of oscillation and overshoot (inverse response) is exhibited at higher operating pressure as a response to the step change of operating flow rate, while a lower operating pressure has yielded a slower response. This is because of the combined and concurrent impact of the higher inlet feed flow rate and a higher applied pressure. Both of these factors are working together to reduce the solute concentration along the feed channel. This can be compared to the case of using a lower feed pressure and a higher feed flow rate conditions. Therefore, it is expected that the average retentate concentration response will be faster and without overshoot in case of using very low operating pressures.

Moreover, Fig. 10 shows an inverse response of the average retentate concentration, where it firstly shows an increase followed by a significant decrease. The first increase is attributed to increasing the feed flow rate, which is commensurate with a higher velocity that reduces the residence time of the brine inside the medium and raises the average retentate concentration. However, the rate of concentration polarization is reduced with the operation time, which is commensurate with increasing the mass transfer coefficient that readily reduces the retentate concentration inside the module.

Fig. 11 readily confirms that using high inlet feed pressures results in markedly noticeable reduction in the average permeate concentration than using low inlet feed pressure conditions. This might be attributed to an increase in the water flux caused by the high inlet feed pressure. Interestingly, Fig. 11 shows that the average permeate concentration is inversely and slightly increased at low operating feed pressures compared to other feed pressures. This phenomenon can be attributed to the use of low operating pressure (lower water flux) in addition to an increase in the frictional pressure drop caused by increasing the

operating feed flow rate. This decreases the advantage of osmotic pressure drop, which lastly reduces the extent of water flux and rises the concentration of permeate side. Thus, the rejection parameter decreases evidenced in Fig. 12. The use of high inlet feed flow rate and high inlet pressure causes a decrease in the average permeate concentration (Fig. 11) and an increase in the solute rejection (Fig. 12).

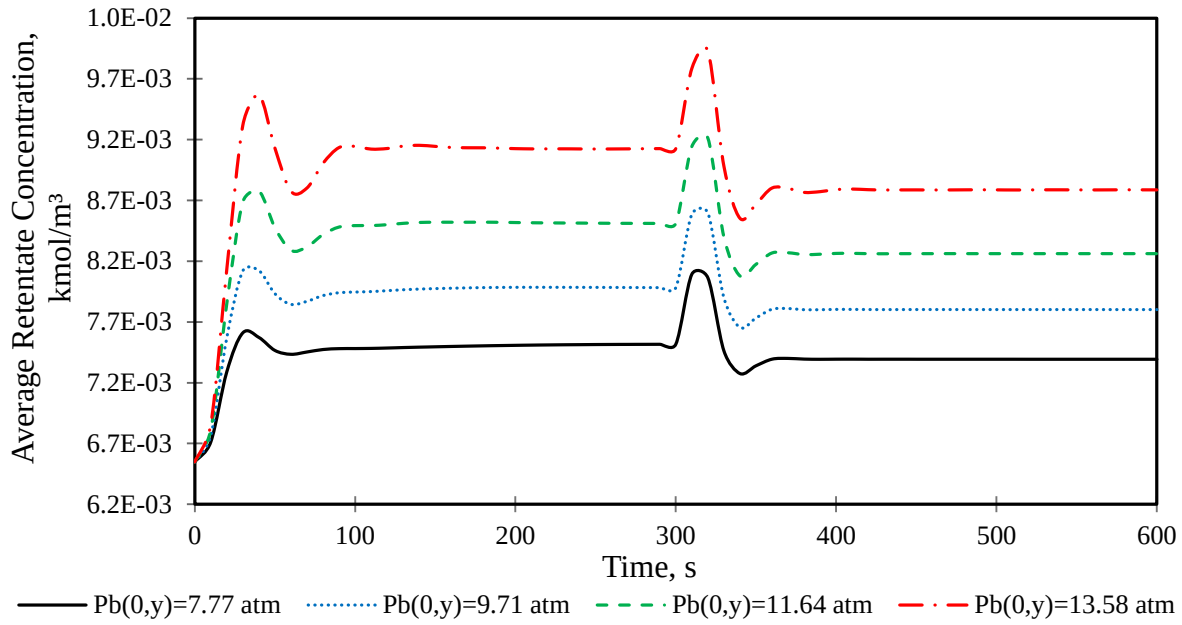

Fig. 10. The influence of the step change of operating feed flow rate on retentate concentration for several operating pressures at operating conditions of 6.548×10^{-3} kmol/m³, 2.33×10^{-4} m³/s and 31.5 °C

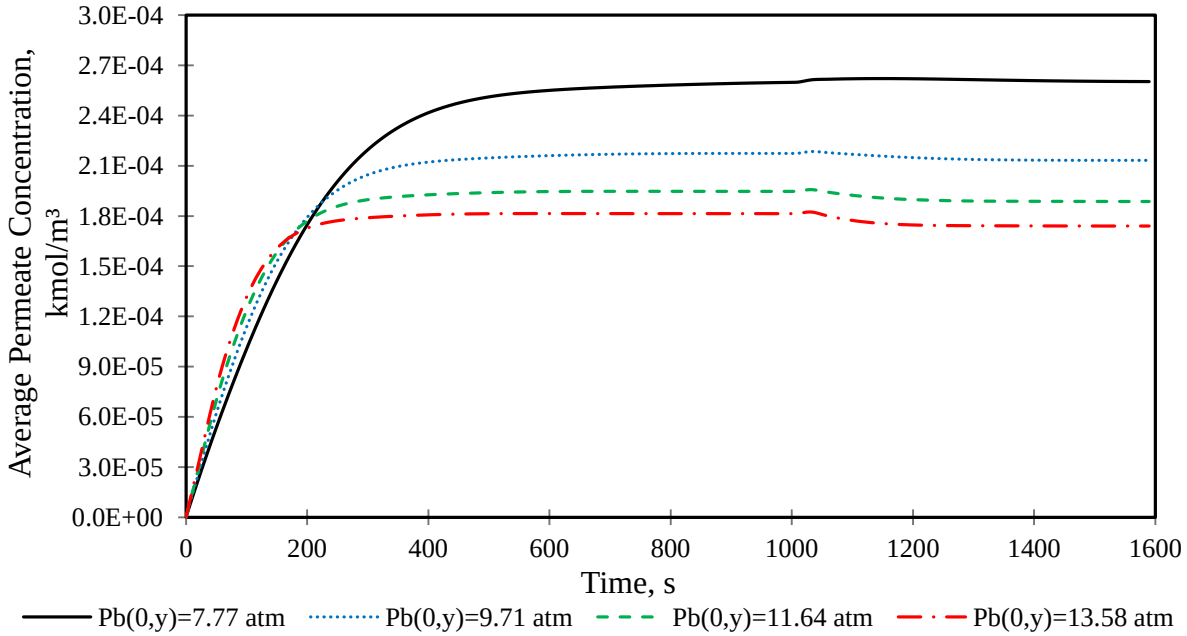

Fig. 11. The influence of the step change of operating feed flow rate on average permeate concentration for several operating pressures at operating conditions of $6.548x10^{-3}$ kmol/m³, $2.33x10^{-4}$ m³/s and 31.5 °C

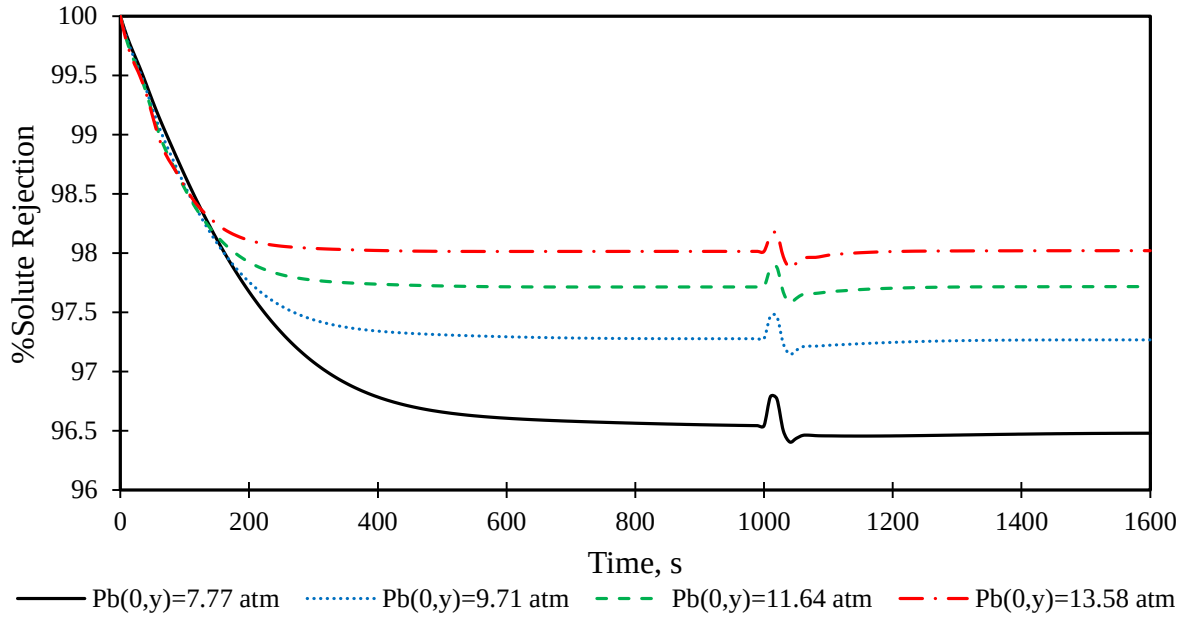

Fig. 12. The influence of the step change of operating feed flow rate on rejection parameter for several operating pressures at operating conditions of $6.548x10^{-3}$ kmol/m³, $2.33x10^{-4}$ m³/s and 31.5 °C

Figs. 13, 14 and 15 show the response of the process for a ramp change of upward increase in the operating flow rate at constant other parameters, which is basically carried out for a period of time with different slops. Up to t = 500 s, the inlet feed flow rate was $2.166x10^{-4}$ m³/s and is increased to $4x10^{-4}$ m³/s and $7x10^{-4}$ m³/s at 500 and 1000 s respectively. While, Fig. 13 is intentionally drawn with different time axes than in Figs. 14 and 15 so as to show the impact of the step change in a clearer way on the specific parameters.

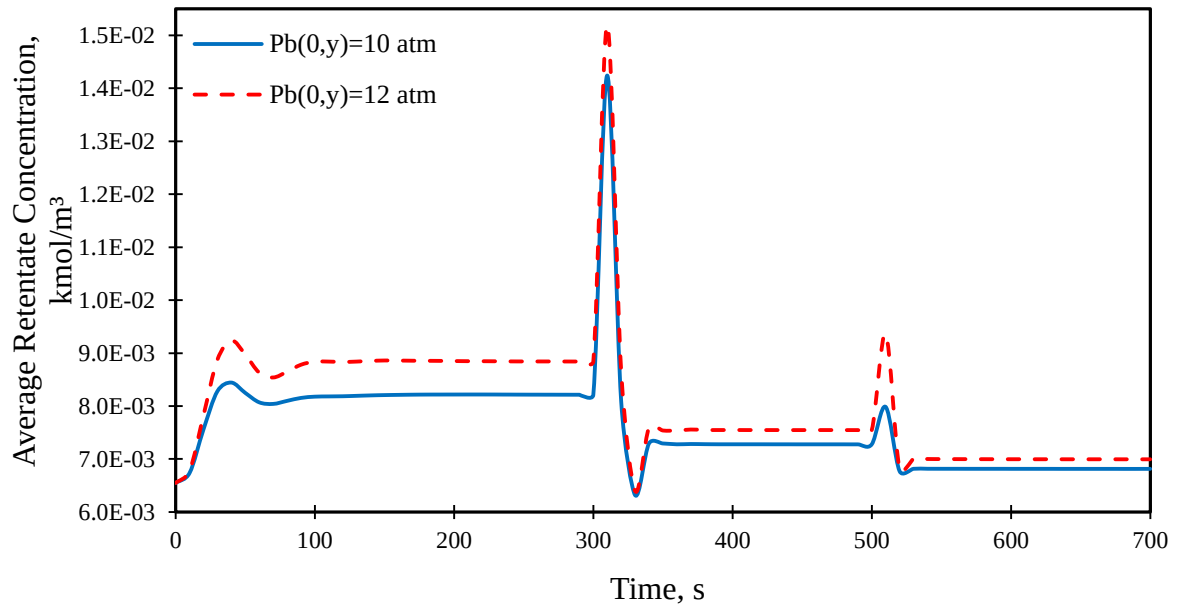

Fig. 13. The result of the ramp change of feed flow rate on retentate concentration for operating conditions of $6.548x10^{-3}$ kmol/m³, 2.166E-4 m³/s, 10 atm and 31.5 °C

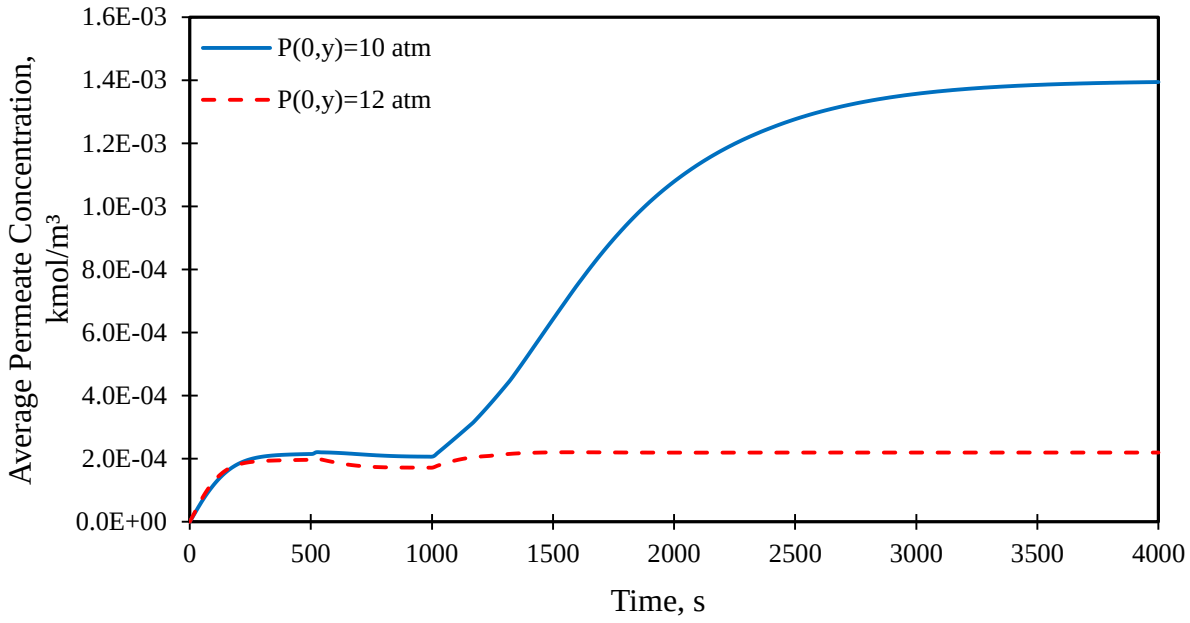

Fig. 14. The result of the ramp change of feed flow rate on average permeate concentration for operating conditions of $6.548x10^{-3}$ kmol/m³, $2.166x10^{-4}$ m³/s, 10 atm and 31.5 °C

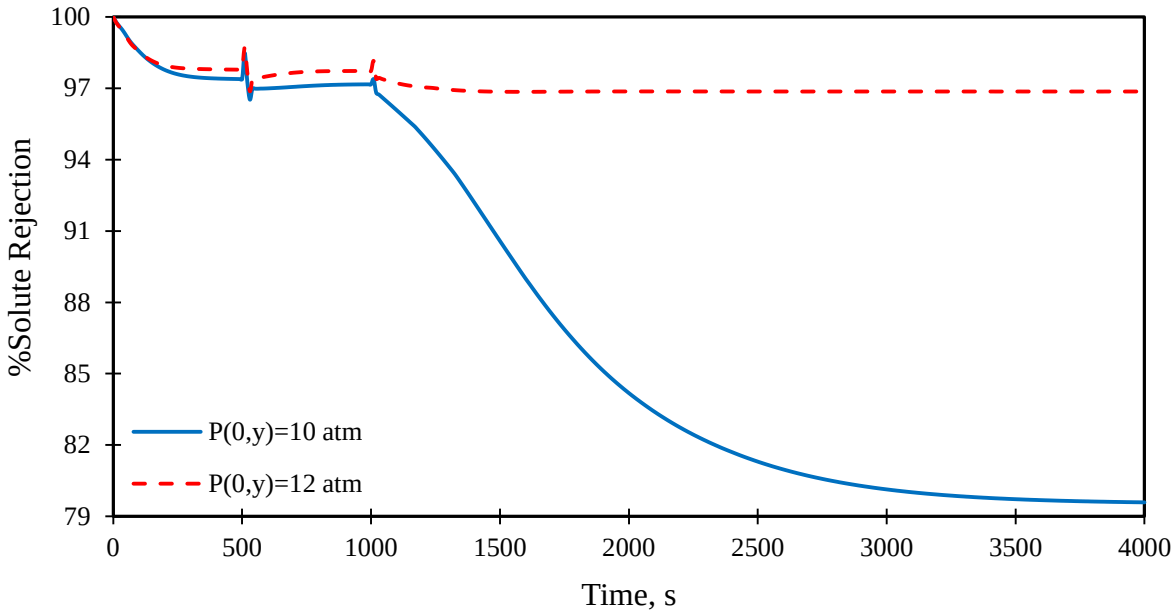

Fig. 15. The result of the ramp change of feed flow rate on solute rejection for operating conditions of $6.548x10^{-3}$ kmol/m³, $2.166x10^{-4}$ m³/s, 10 atm and 31.5 °C

Fig. 13 shows that a considerable overshoot followed by an inverse response occurs after increasing the operating flow rate by about 84 % from $2.166x10^{-4}$ m³/s to $4x10^{-4}$ m³/s. However, the second ramp change has shown a low degree of response after increasing the operating flow rate by 75 % from $4x10^{-4}$ m³/s to $7x10^{-4}$ m³/s. This behaviour can be explained by increasing the rate of disturbance instantaneously, which observed a longer shoot response. While, increasing the feed flow rate at recent high feed flow rate is commensurate with a lower rate of disturbance that reflects a lower shoot response.

Fig. 13 confirms that increasing the operating pressure can raise the retentate concentration due to increasing the level of water penetration. Interestingly, Figs. 14 and 15 shows that the process requires a longer time to be settled after imposing the second ramp change to access the higher feed flow rate of $7x10^{-4}$ m³/s at medium operating pressure of 10 atm. This is clear in the response of both the average permeate concentration and solute rejection compared to the response of operating pressure of 12 atm. Also, the process shows a remarkable decrease in the solute rejection at operating pressure of 10 atm compared with a slight change at 12 atm. It is expected that the concurrence of high feed flow rate and medium pressure is the main reason of this fluctuation, where the 10 atm was not able to retrieve the deterioration of solute rejection caused at high feed flow rate. However, it seems that the operating pressure of 12 atm has improved the solute rejection albeit keeping the rejection at approximately constant value.

5.3 The inlet feed concentration

The impact of the step change of the operating concentration on the average retentate concentration, average permeate concentration and rejection parameter under several operating pressures with constant operating feed flow rate and temperature can be shown in Figs. 16 to 18. Up to t = 1000 s, the inlet feed concentration is $0.819x10^{-3}$ kmol/m³ and at t = 1000 s, the inlet feed concentration is achieved to $6.548x10^{-3}$ kmol/m³. Note that, Fig. 16 is intentionally drawn with different time axes than in Figs. 17 and 18 so as to show the impact of the step change in a clearer way on the specific parameters.

As expected, the increase of the inlet feed concentration raises the average retentate concentration, which results in a higher osmotic pressure and average permeate concentration and lower water flux.

Interestingly, the system spends more time to achieve its steady state in comparison to a step change in the inlet feed pressure and feed flow rate. This might be qualified to the growth in the degree of instability throughout the step change of the inlet feed concentration. Similarly, the system with lower feed pressure conditions needs more time to settle in comparison to higher inlet feed pressure conditions (Figs. 17 and 18). This is due to a lower water flux occurring inside the permeate channel when using lower feed pressures, which needs more time to get a constant value of solute concentration at the permeate channel in comparison to higher feed pressures. Higher feed pressure is convoyed to a higher degree of permeation, which enables a steady average permeate concentration faster than applying low inlet feed pressure conditions. Indeed, Fig. 18 shows that the solute rejection growths because of an increase in the operating concentration as a result to a growth of the strength of membrane rejection.

Fig. 18 shows a strong overshoot of the relation of the rejection parameter for a step change in the operating concentration. It is probable that this is a consequence of the influence of the solute concentration on the feed side (Fig. 16). Fig. 18 shows that operating at high pressures yields better solute rejection with lower salt concentration of the permeate in comparison to that by lower pressures. This is because of a reduction in the water flux due to a reduction in the operating pressure, which hinders the rejection parameter.

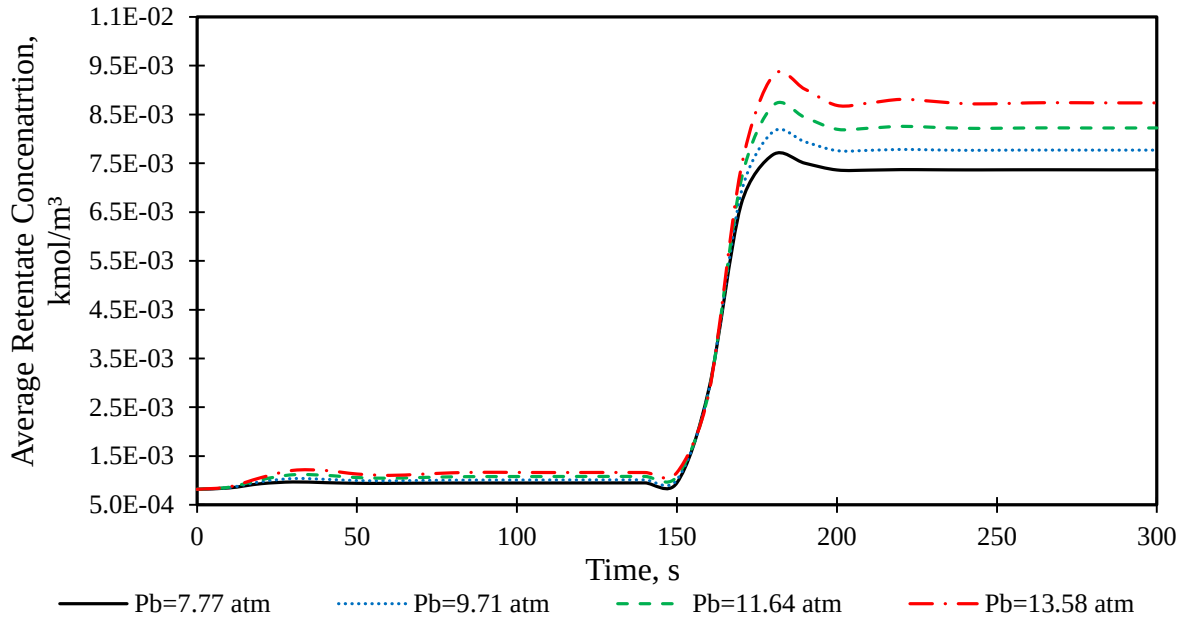

Fig. 16. The result of the step change of operating concentration on retentate concentration for several operating pressures at operating conditions of 2.583×10^{-4} m³/s, 0.819×10^{-3} kmol/m³ and 31.5 °C

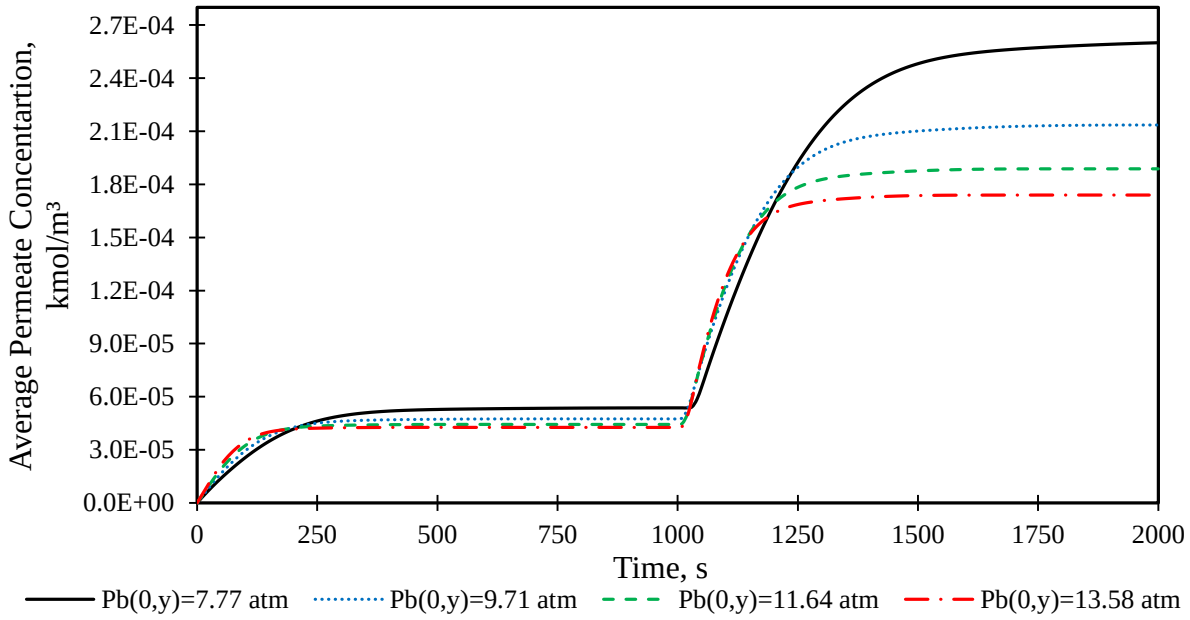

Fig. 17. The result of the step change of operating concentration on average permeate concentration for several operating pressures at operating conditions of 2.583×10^{-4} m³/s, 0.819×10^{-3} kmol/m³ and 31.5 °C

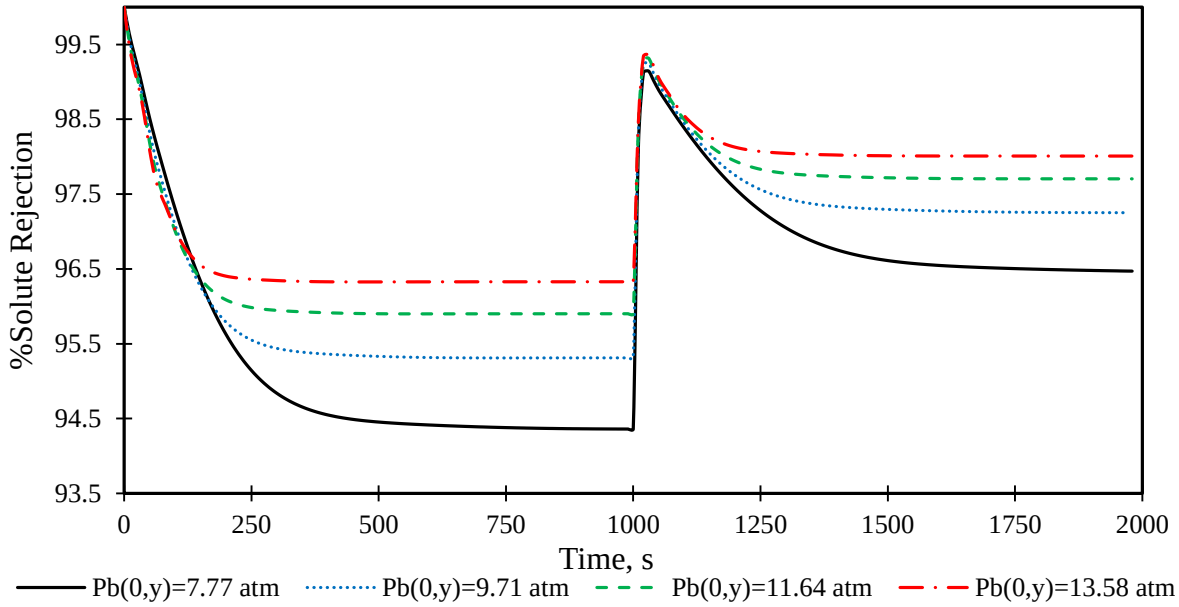

Fig. 18. The result of the step change of operating concentration on rejection parameter for several operating pressures at operating conditions of 2.583×10^{-4} m³/s, 0.819×10^{-3} kmol/m³ and 31.5 °C

5.4 The inlet feed temperature

Figs. 19 to 21 show the response of the step change of the operating temperature on the average retentate concentration, average permeate concentration and rejection for several operating pressures with constant operating feed flow rate and concentration. Up to t = 1000 s the inlet feed temperature was 31.5 ºC and at t = 1000 s, the operating temperature is increased to 40 ºC. Note that, Fig. 19 is intentionally drawn with different time axes than in Figs. 20 and 21 so as to show the impact of the step change in a clearer way on the specific parameters.

Interestingly, the process requires a longer time to settle after imposing a step change in the operating temperature.

Obviously, increasing the operating temperature will lead to a rise in the viscosity parameter, which reduces the concentration polarisation impact and causes an increase in the passage of water. That in turn leads to an increase of the retentate concentration (Fig. 19) and a reduction of the average permeate concentration (Fig. 20). In addition, increasing operating pressure will increase the average retentate concentration and reduces the average permeate concentration. This, the solute rejection rises because of an increase in the operating temperature (Fig. 21).

It is not complicated to see that the average retentate concentration, average permeate concentration and the solute rejection are exhibiting underdamped responses whithout clear

overshoots before getting its steady state as a response to step change of operating temperature and compared with the previous tested cases. However, the same behaviour has been solely noticed for average permeate concentration after imposing the step change of operating pressure, concentration and flow rate. This can be explained by the lower disturbance that can ocur after supplying a step change of temperature from 31.5 ºC to 40 ºC, compared with a higher degree of disturbance that is expected to occur at other step changes of operating parameters.

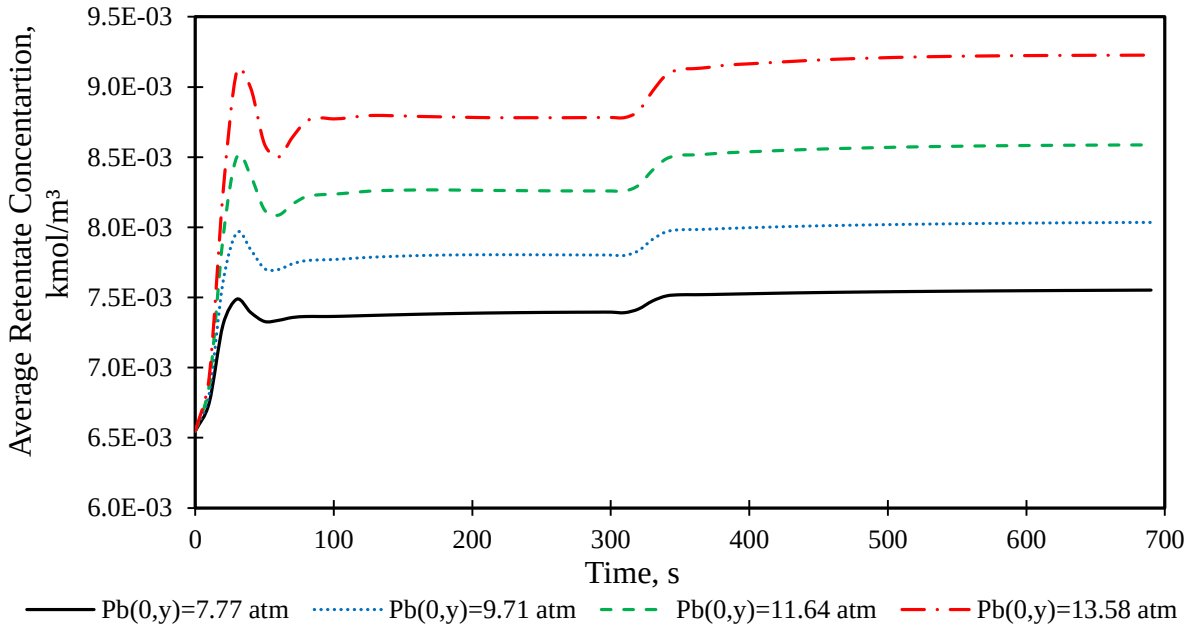

Fig. 19. The result the step change of operating temperature on retentate concentration for several operating pressures at operating conditions of 2.583x10^{-4} m³/s, 6.548x10 $^{-3}$ kmol/m³ and 31.5 ºC

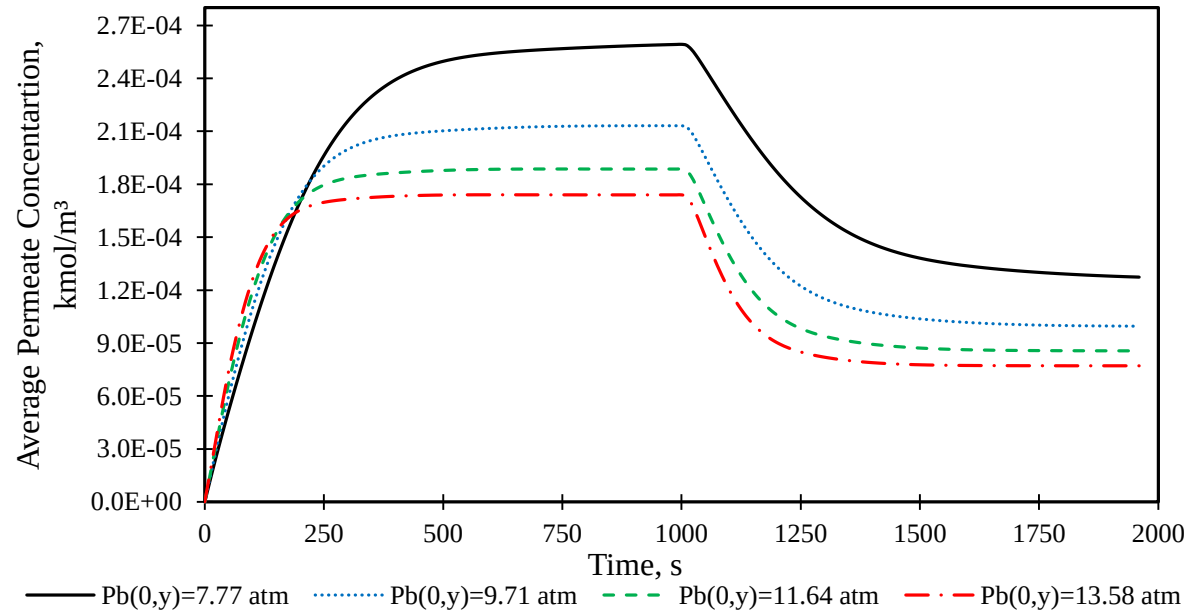

Fig. 20. The effects of the step change in operating temperature to mean permeate concentration for several operating pressures at operating conditions of 2.583×10^{-4} m³/s, 6.548×10^{-3} kmol/m³ and 31.5 ºC

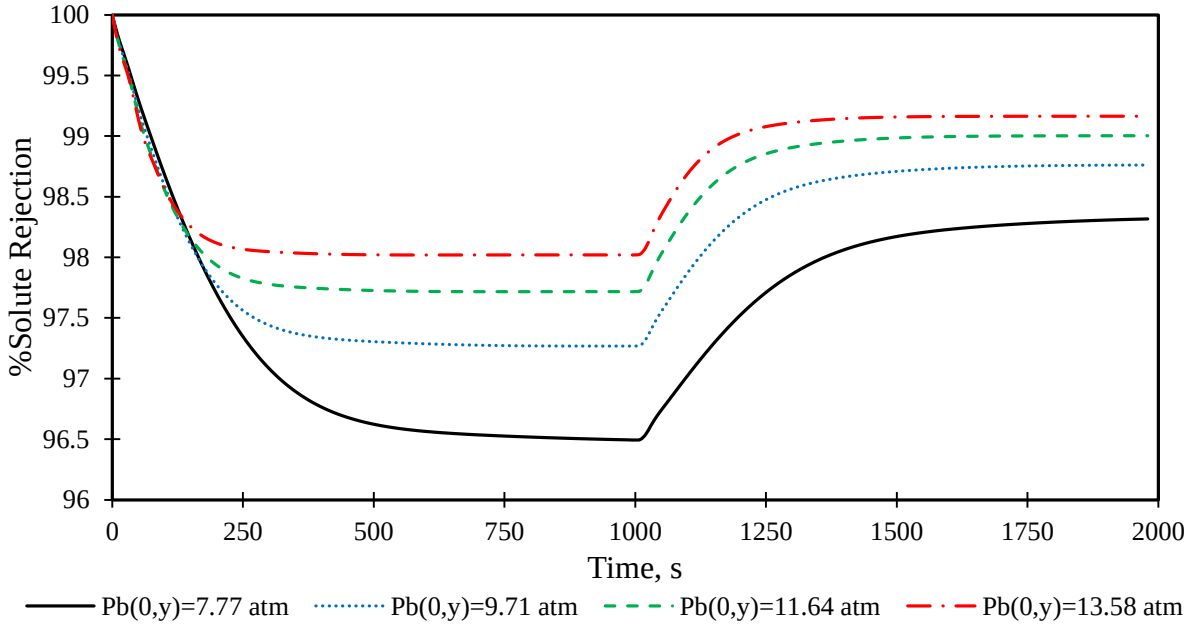

Fig. 21. The result of the step change of operating temperature on rejection parameter for several operating pressures at operating conditions of 2.583×10^{-4} m³/s, 6.548×10^{-3} kmol/m³ and 31.5 ºC

It is clear from the above dynamic simulation results that the process requires a specific time to be settled after imposing a step change on the operating parameters, which is mainly dependent on the type of input parameters. In addition, it is noticed that the tested parameters at the feed channel such as retentate concentration is settled faster than parameters of permeate channel such as permeate concentration. This is due to a high degree of disturbance that occurs in the feed channel compared to permeate channel. Therefore, the permeate concentration requires more time to be settled due to its consistent relation to water flux that is already varied along the feed axis. Most importantly, the combined step change of operating concentration and temperature expenses a longer time to settle the process performance than that of the combined step change of the feed pressure and feed flow rate. Such disturbances often occur in usual feed water sources, due to sequential and spatial variations. From a practical aspect, it seems that such step change can occur as a result of a number of reasons, including an instant increase in the feed concentration, pump fault, and the season variation. As a result, the process performance is likely to be affected as a response to a step change, which might occur in the operating conditions. In other words, the process will fluctuate as a response to this change until it settles at a constant value. Having said this, the requirements of gaining a new steady state operation process is mainly

associated with the measurements of the system and the weight of the stepwise. Interestingly, the model reported in this paper was capable to provide a clear insight of the time required to gain a new steady state after applying a step change of operating parameters. Once the RO process performance (rejection and recovery rate) against the operating conditions is determined and the changes as a function of time are defined, a control system can be employed in order to operate correctly the system. To exemplify, once the proper optimal permeate concentration of dimethylphenol is determined as a set-point, the dynamic model developed will be used to dynamically simulate the process. Then, the logic of the adaptive controller will be set to follow the simulation and to react any fluctuated response in a way by setting back the set-point value. Consequently, the use of an automatic control for the wastewater RO process is both critical and important for maintaining process performance within a specified level. The control efficiency of different types of controller scheme such as PID (proportional–integral–derivative) and MPC (Model predictive control) has to be examined for the wastewater RO process taking into consideration a constant performance of organic compound removal (lower release of pollutants to the environment) under a realistic water recovery. Additionally, one of the advantages of the advanced control system is to maintain a lower permeate recovery with the lowest operating pressure in order to reduce the operation cost and prolong the membrane life. In this aspect, several contributions have been made in the literature to process control of the seawater RO desalination systems. Having said this, it seems that there is a necessity of investigating the proper control system for the removal of high-toxic compounds (such as dimethylphenol) from wastewater.

6. Conclusions

In this work an RO process is considered for the removal of pollutants such as dimethylphenol from wastewater. For a given configuration (design) of the process, a number of operating parameters affect the process performance. While the ultimate goal would be to design effective and efficient controllers for such process, understanding the dynamics of such process is no doubt a pre-step which is the focus of this study. Therefore, a two-dimensional dynamic modelling platform for the RO process with a spiral wound membrane has been developed extending our earlier 2-D steady state model and tested for the removal of dimethylphenol in wastewater. A comparative study between the 2-D model and a 1-D model has been presented to justify the use of the 2-D model for further study of the RO process.

The 2-D can be easily extended for testing other pollutants by simply embedding physical property models of relevant pollutant into the model platform. The proposed model can estimate the dynamic behaviour of the operating parameters at any dimensions of the membrane length and width regarding the operating time compared to the 1-D model. Besides, this model readily facilitates the estimation of the dynamic behaviour of water and solute fluxes in addition to solute concentration at the membrane wall. The proposed model allows a better understanding of the impact of the mass transfer coefficient and concentration polarisation variation in both dimensions of the module. The dynamic simulation of the 2-D modelling has facilitated the investigation of the impact of a step change of the operating parameters on the performance of the whole system. The dynamic simulation results show that the process requires a specific time to settle after imposing a step change on a number of operating parameters. Having said this, the settling time is dependent on the type of the operating parameters. Specifically, the operating concentration and temperature step changes expense longer time to settle the process than the operating pressure and flow rate.

Nomenclature

A_m : The membrane area (m^2)

A_w : Permeate transport parameter (m/atm s)

B_s : Solute transport parameter (m/s)

b : Friction parameter at feed and permeate channels (atm s/m^4)

C_b : Solute concentration in the feed side ($kmol/m^3$)

$C_{b(inlet)}$: Inlet solute concentration ($kmol/m^3$)

$C_{b(outlet)}$: Retentate concentration ($kmol/m^3$)

C_m : Dimensionless solute concentration

C_w : Membrane wall solute concentration ($kmol/m^3$)

C_p : Solute concentration in the permeate side ($kmol/m^3$)

D_b : Diffusivity parameter of feed (m^2/s)

D_p : Diffusivity parameter of permeate (m^2/s)

d_{ef} : Corresponding diameter of permeate channel (m)

d_{ep} : Corresponding diameter of feed channel (m)

F_b : Feed flow rate on the feed channel (m^3/s)

$F_{b(inlet)}$: Inlet feed flow rate (m^3/s)

$F_{b(outlet)}$: Retentate flow rate (m^3/s)

F_p : Permeate flow rate on the permeate channel (m^3/s)

F_s : Solute molar flux in x-axis ($kmol/m^2\ s$)

J_s : Solute molar flux ($kmol/m^2\ s$)

J_w : Water flux through the membrane (m/s)

k : Solute mass transfer coefficient (m/s)

L : Membrane length (m)

P_p : Permeate pressure on the permeate side (atm)

P_b : Feed pressure on the feed channel (atm)

$P_{b(inlet)}$: Inlet feed pressure (atm)

R : Gas low constant $\left(\mathrm{R} = 0.082 \frac{\mathrm{atm\ m^3}}{\mathrm{K\ kmol}}\right)$

Re_b : Reynolds number of the feed (dimensionless)

$Rej_{(av)}$: Average solute rejection parameter of the unit (dimensionless)

$Rec_{(Total)}$: Total permeate recovery rate (dimensionless)

Re_p : Reynolds number of the permeate (dimensionless)

T_b : Operating feed temperature (°C)

t_f : Thickness of feed spacer (m)

T_p : Permeate temperature on the permeate channel (°C)

t_p : Thickness of permeate spacer (m)

W : Membrane width (m)

Symbols

ρ_b : Density parameter of feed (kg/m^3)

ρ_p : Density parameter of permeate (kg/m^3)

ρ_w : Molal density of water (55.56 $kmol/m^3$)

Δx : Length of each sub-section in x-axis (m)

Δy : Width of sub-section in y-axis (m)

μ_b : Viscosity parameter of feed (kg/m s)

μ_p : Viscosity parameter of permeate (kg/m s)

References

Ahmad A. L., Chong M. F. and Bhatia S., 2007. Mathematical modeling of multiple solutes system for reverse osmosis process in palm oil mill effluent (POME) treatment. *Chemical Engineering Journal*, 132, 183-193.

Al-Obaidi M. A. and Mujtaba I. M., 2016. Steady state and dynamic modeling of spiral wound wastewaterreverse osmosis process. *Computers and Chemical Engineering*, 90, 278-299.

Al-Obaidi M. A., Kara-Zaïtri C. and Mujtaba I. M., 2017. Wastewater treatment by spiral wound reverse osmosis: Development and validation of a two-dimensional process model. *Journal of Cleaner Production* 140, 1429-1443.

Avlonitis S., Hanbury W. T. and Boudinar M. B., 1991. Spiral wound modules performance. An analytical solution, part I. *Desalination*, 81 (1-3), 191-208.

Avloniti S., Hanbury W. T. and Boudinar M. B., 1993. Spiral wound modules performance an analytical solution: Part II. *Desalination*, 89 (3), 227-246.

Avlonitis S. A., Pappas M. and Moutesidis K., 2007. A unified model for the detailed investigation of membrane modules and RO plants performance. *Desalination*, 203 (1-3), 218-228.

Bartman A. R., Christofides P. D., and Cohen Y., 2009. Nonlinear Model-Based Control of an Experimental Reverse-Osmosis Water Desalination System. *Ind. Eng. Chem. Res.*, 48, 6126-6136.

Bartman A. R., Zhu A., Christofides P. D., and Cohen Y., 2010. Minimizing energy consumption in reverse osmosis membrane desalination using optimization-based control. *Journal of Process Control*, 20, 1261-1269.

Boudinar M. B., Hanbury W. T., and Avlonitis S., 1992. Numerical simulation and optimisation of spiral-wound modules. *Desalination*, 86 (3), 273-290.

Chen-Jen Lee, Chen Y. S. and Wang G. -B., 2010. A dynamic simulation model of reverse osmosis desalination systems. The 5th International Symposium on Design, Operation and Control of Chemical Processes, PSE ASIA, Singapore.

Fritzmann C., Löwenberg J., Wintgens T. and Melin T., 2007. State-of-the-art of reverse osmosis desalination. *Desalination*, 216, 1-76.

Fujioka T., Khan S. J., Mcdonald J. A., Roux A., Poussade Y., Drewes J. E. and Nghiem L. D., 2014. Modelling the rejection of N-nitrosamines by a spiral-wound reverse osmosis system: Mathematical model development and validation. *Journal of Membrane Science*, 454, 212-219.

Geraldes V., Pereira N. E., and Norberta de Pinho M., 2005. Simulation and Optimization of Medium-Sized Seawater Reverse Osmosis Processes with Spiral-Wound Modules. *Industrial and Engineering Chemistry Research*, 44 (6), 1897-1905.

Goh P. S., Matsuura T., Ismail A. F., Hilal N., 2016. Recent trends in membranes and membrane processes for desalination. *Desalination,* 391, 43-60.

Gómez J., León G., Hidalgo A., Gómez M., Murcia M. and Griñán G., 2009. Application of reverse osmosis to remove aniline from wastewater. *Desalination,* 245, 687-693.

Gu B., Xu X. Y., and Adjiman C. S., 2017. A predictive model for spiral wound reverse osmosis membranemodules: The effect of winding geometry and accurate geometric details. *Computers and Chemical Engineering*, 96, 248-265.

Li. M., 2012. Optimal plant operation of brackish water reverse osmosis (BWRO) desalination. *Desalination,* 293, 61-68.

Mane P. P., Park P. -K., Hyung H., Brown J. C. and Kim J. -H., 2009. Modeling boron rejection in pilot- and full-scale reverse osmosis desalination processes. *Journal of Membrane Science*, 338, 119-127.

Marriott J., and Sørensen, E., 2003. A general approach to modelling membrane modules. *Chemical Engineering Science*, 58 (22) 4975-4990.

Oh H.-J., Hwang T.-M. and Lee S., 2009. A simplified simulation model of RO systems for seawater desalination. *Desalination*, 238, 128-139.

Process System Enterprise Ltd., 2001. gPROMS Introductory User Guide. London: Process System Enterprise Ltd.

Sagne C., Fargues C., Broyart B., Lameloise M.-L. and Decloux M., 2009. Modeling permeation of volatile organic molecules through reverse osmosis spiral-wound membranes. *Journal of Membrane Science,* 330, 40-50.

Senthilmurugan S., Ahluwalia A., and Gupta S. K., 2005. Modeling of a spiral-wound module and estimation of model parameters using numerical techniques. *Desalination,* 173(3),269-286.

Singh V., Jain P. K. and Das C., 2013. Performance of spiral wound ultrafiltration membrane module for with and without permeate recycle: Experimental and theoretical consideration. *Desalination,* 322, 94-103.

Spiegler K. S. and Kedem O., 1966. Thermodynamics of hyperfiltration (reverseosmosis): criteria for efficient membranes. *Desalination* 1, 311-326.

Srinivasan G., Sundaramoorthy S. and Murthy D. V. R., 2011. Validation of an analytical model for spiral wound reverse osmosis membrane module using experimental data on the removal of dimethylphenol. *Desalination,* 281**,** 199-208.

Sundaramoorthy S., Srinivasan G. and Murthy D. V. R., 2011a. An analytical model for spiral wound reverse osmosis membrane modules: Part I- Model development and parameter estimation. *Desalination*, 280**,** 403-411.

Sundaramoorthy S., Srinivasan G. and Murthy D. V. R., 2011b. An analytical model for spiral wound reverse osmosis membrane modules: Part II- Experimental validation. *Desalination*, 277, 257-264.

Appendix (A)

Table A.1. The dynamic model equations (Al-Obaidi *et al.*, 2017)

No	Title	The Mathematical Expression
1	Dynamic axial and vertical water flux	$\frac{dJ_{w(x,y)}}{dt} = \left\{\left(A_w\left((P_{b(x,y)} - P_{p(x,y)}) - RT_{b(x,y)}(C_{w(x,y)} - C_{p(x,y)})\right)\right) - J_{w(x,y)}\right\}\left(\frac{F_{b(x,y)}}{t_f\,\Delta x\,\Delta y}\right)$
2	Dynamic axial and vertical solute flux	$\frac{dJ_{s(x,y)}}{dt} = \left\{\left(B_s \exp\left(\frac{J_{w(x,y)}}{k_{(x,y)}}\right)(C_{b(x,y)} - C_{p(x,y)})\right) - J_{s(x,y)}\right\}\left(\frac{F_{b(x,y)}}{t_f\,\Delta x\,\Delta y}\right)$
3	Dynamic axial and vertical membrane wall concentration	$\frac{dC_{w(x,y)}}{dt} = \left\{\left(C_{p(x,y)} + \exp\left(\frac{J_{w(x,y)}}{k_{(x,y)}}\right)(C_{b(x,y)} - C_{p(x,y)})\right) - C_{w(x,y)}\right\}\left(\frac{F_{b(x,y)}}{t_f\,\Delta x\,\Delta y}\right)$
4	Pressure difference along the two dimensions of the membrane	$\Delta P_{b_{(x,y)}} = (P_{b(x,y)} - P_{p(x,y)})$
5	Dynamic axial and vertical feed flow rate	$\frac{dF_{b(x,y)}}{dt} = \left\{[-(\Delta y)(J_{w(x,y)})] - \left(\frac{dF_{b(x,y)}}{dx}\right)\right\}\left\{\frac{F_{b(x,y)}}{t_f\,\Delta y}\right\} + \left\{[-(\Delta x)(J_{w(x,y)})] - \left(\frac{dF_{b(x,y)}}{dy}\right)\right\}\left\{\frac{F_{b(x,y)}}{t_f\,\Delta x}\right\}$
6	Dynamic axial and vertical feed pressure	$\frac{dP_{b(x,y)}}{dt} = \left[\left[\left((-b\,F_{b(x,y)})\right)\left(\frac{F_{b(x,y)}}{\Delta x\ t_f}\right)\right] - \left[\left(\frac{dP_{b(x)}}{dx}\right)\left(\frac{F_{b(x,y)}}{\Delta y\,t_f}\right)\right] - \left[\left(\frac{dP_{b(y)}}{dy}\right)\left(\frac{F_{b(x,y)}}{\Delta x\ t_f}\right)\right]\right]$
7	Dynamic axial and vertical permeated pressure	$\frac{dP_{p(x,y)}}{dt} = \left[\left[\left((-b\,F_{p(x,y)})\right)\left(\frac{F_{p(x,y)}}{\Delta y\,t_p} + \frac{F_{p(x,y)}}{\Delta x\ t_p}\right)\right] - \left[\left(\frac{dP_{p(x,y)}}{dx}\right)\left(\frac{F_{p(x,y)}}{\Delta y\,t_p}\right)\right] - \left[\left(\frac{dP_{p(x,y)}}{dy}\right)\left(\frac{F_{p(x,y)}}{\Delta x\ t_p}\right)\right]\right]$
8	Axial and vertical permeated flow rate	$F_{p(x,y)} = J_{w(x,y)}\,\Delta x\,\Delta y$
9	Dynamic axial and vertical molar flux of feed	$\frac{dC_{b(x,y)}}{dt} = -\frac{C_{b(x,y)}}{t_f\,\Delta y}\frac{dF_{b(x,y)}}{dx} - \frac{F_{b(x,y)}}{t_f\,\Delta y}\frac{dC_{b(x,y)}}{dx} + \frac{d}{dx}\left[D_{b(x,y)}\frac{dC_{b(x,y)}}{dx}\right] - \frac{C_{b(x,y)}}{t_f\,\Delta x}\frac{dF_{b(x,y)}}{dy} - \frac{F_{b(x,y)}}{t_f\,\Delta x}\frac{dC_{b(x,y)}}{dy} + \frac{d}{dy}\left[D_{b(x,y)}\frac{dC_{b(x,y)}}{dy}\right] - \frac{J_{s(x,y)}}{t_f}$
10	Dynamic axial and vertical molar flux of permeate	$\frac{dC_{p(x,y)}}{dt} = -\frac{C_{p(x,y)}}{t_f\,\Delta y}\frac{dF_{p(x,y)}}{dx} - \frac{F_{p(x,y)}}{t_f\,\Delta y}\frac{dC_{p(x,y)}}{dx} + \frac{d}{dx}\left[D_{p(x,y)}\frac{dC_{p(x,y)}}{dx}\right] - \frac{C_{p(x,y)}}{t_f\,\Delta x}\frac{dF_{p(x,y)}}{dy} - \frac{F_{p(x,y)}}{t_f\,\Delta x}\frac{dC_{p(x,y)}}{dy} + \frac{d}{dy}\left[D_{p(x,y)}\frac{dC_{p(x,y)}}{dy}\right] + \frac{J_{s(x,y)}}{t_f}$
11	Dynamic axial and vertical feed temperature	$\frac{dT_{b(x,y)}}{dt} = \left[\frac{F_{b(x,y)}\,(T_{b(x-1,y)} - T_{b(x,y)})}{t_f\,\Delta x\,\Delta y}\right] - \left[\frac{J_{w(x,y)}\,(T_{b(x,y)} - T_{p(x,y)})}{t_f}\right]$
12	Dynamic axial and vertical permeated temperature	$\frac{dT_{p(x,y)}}{dt} = \left[\frac{J_{w(x,y)}\,(T_{b(x,y)} - T_{p(x,y)})}{t_f}\right]$
13	Total permeated flow rate	$F_{p(Total)} = \sum F_{p(x,y)}$
14	Total water recovery	$Rec_{(Total)} = \frac{F_{p(Total)}}{F_{b(0,y)}} x100$

15	Average solute rejection	$\mathrm{Rej}_{(av)} = \frac{C_{b(x=L,y)} - C_{p(av)}}{C_{b(x=L,y)}} x100$
16	Average permeated concentration	$C_{p(av)} = \sum C_{p(x,y)} / n.\,sub - divisions$
17	Axial and vertical mass transfer coefficient	$k_{(x,y)}\, de_b = 246.9\, D_{b(x,y)}\ \mathrm{Re}_{b(x,y)}^{0.101}\ \mathrm{Re}_{p(x,y)}^{0.803}\ C_{m(x,y)}^{0.129}$
18	Axial and vertical dimensionless solute concentration	$C_{m(x,y)} = \frac{C_{b(x,y)}}{\rho_w}$
19	Axial and vertical feed diffusivity	$D_{b(x,y)} = 6.725x10^{-6} \exp\left\{0.1546x10^{-3}\, C_{b(x,y)}\, x18.01253 - \frac{2513}{T_{b(x,y)}+273.15}\right\}$

Table A.1. The dynamic model equations (continued)

No	Title	The Mathematical Expression
20	Axial and vertical permeated diffusivity	$D_{p(x,y)} = 6.725x10^{-6} \exp\left\{0.1546x10^{-3}\, C_{p(x,y)} x18.01253 - \frac{2513}{T_{p(x,y)}+273.15}\right\}$
21	Axial and vertical feed viscosity	$\mu_{b(x,y)} = 1.234x10^{-6} \exp\left\{0.0212\, C_{b(x,y)}\, x18.0153 + \frac{1965}{T_{b(x,y)}+273.15}\right\}$
22	Axial and vertical permeated viscosity	$\mu_{p(x,y)} = 1.234x10^{-6} \exp\left\{0.0212\, C_{p(x,y)}\, x18.0153 + \frac{1965}{T_{p(x,y)}+273.15}\right\}$
23	Axial and vertical feed density	$\rho_{b(x,y)} = 498.4\, m_{f(x,y)} \sqrt{\left[248400\, m_{f(x,y)}^2 + 752.4\, m_{f(x,y)}\, C_{b(x,y)}\, x18.0153\right]}$
24	Axial and vertical permeated density	$\rho_{p(x,y)} = 498.4\, m_{p(x,y)} \sqrt{\left[248400\, m_{p(x,y)}^2 + 752.4\, m_{p(x,y)}\, C_{p(x,y)}\, x18.0153\right]}$
25	Axial and vertical variable in Eq. (24)	$m_{f(x,y)} = 1.0069 - 2.757x10^{-4}\, T_{b(x,y)}$
26	Axial and vertical variable in the above Equation	$m_{p(x,y)} = 1.0069 - 2.757x10^{-4}\, T_{p(x,y)}$
27	Axial and vertical feed channel Reynolds number	$\mathrm{Re}_{b(x,y)} = \frac{\rho_{b(x,y)}\, de_b\ F_{b(x,y)}}{t_f\, W\ \mu_{b(x,y)}}$
28	Axial and vertical permeate channel Reynolds number	$\mathrm{Re}_{p(x,y)} = \frac{\rho_{p(x,y)}\, de_p\, J_{w(x,y)}}{\mu_{p(x,y)}}$
29	The equivalent diameter of feed channel	$de_b = 2t_f$
30	The equivalent diameter of permeated channel	$de_p = 2t_p$
	Total number of equation is 30	

Table A.2. Specifications of variables

Items	Total
Variables: $J_{w(x,y)}, J_{s(x,y)}, P_{b(x,y)}, P_{p(x,y)}, T_{b(x,y)}, T_{p(x,y)}, C_{w(x,y)}, C_{b(x,y)}, C_{p(x,y)}, F_{b(x,y)}, F_{p(x,y)}, k_{(x,y)}, F_{p(Total)}, \%Rec_{(Total)}, \%Rej_{(av)}, C_{p(av)}, de_b, de_p, C_{m(x,y)}, D_{b(x,y)}, D_{p(x,y)}, \mu_{b(x,y)}, \mu_{p(x,y)}, \rho_{b(x,y)}, \rho_{p(x,y)}, m_{f(x,y)}, m_{p(x,y)}, \mathrm{Re}_{b(x,y)}, \mathrm{Re}_{p(x,y)}, \Delta P_{b_{(x,y)}}, A_w, B_s, L, W, \rho_w, b, t_f, t_p$ and ρ_w	39
Differential variables at $t = 0$:	10

$\frac{dJ_{w(x,y)}}{dt}, \frac{dJ_{s(x,y)}}{dt}, \frac{dC_{w(x,y)}}{dt}, \frac{dF_{b(x,y)}}{dt}, \frac{dP_{b_{(x,y)}}}{dt}, \frac{dP_{p_{(x,y)}}}{dt}, \frac{dC_{b(x,y)}}{dt}, \frac{dC_{p(x,y)}}{dt}, \frac{dT_{b(x,y)}}{dt}$ and $\frac{dT_{p(x,y)}}{dt}$	
t is independent variable	1
Total	50

The specification of the dynamic model (Table A.2) shows that the total number of variables is 50, while the number of equations is 30 as can be seen in Table A.1, so:
D.F. = Total number of variables – Total number of equations
D.F. = 50 – 30 = 20
The number of parameters is 9 (Table A.3) and assigned initial values of differential variables at $t = 0$ are 10 and independent variable =1, (time, t). So, this specification counts 20 variables.

Table A.3. Specifications of constant parameters and differential variables at t = 0

Parameter	Value
Feed spacer thickness (t_f)	0.8 mm
Permeate channel thickness (t_p)	0.5 mm
Module length (L)	0.934 m
Module width (W)	8.4 m
Molal density of water (ρ_w)	5.56 kmol/m³
Gas law constant (R)	0.082 (atm m³/K kmol)
Feed channel friction parameter (b)	9400.9 $\left(\frac{atm\ s}{m^4}\right)$
Solvent transport coefficient (A_w)	9.42009 x10^{-7} $\left(\frac{m}{atm\ s}\right)$
Solute transport coefficient (B_s) (Dimethylphenol)	2.22577 x10^{-8} $\left(\frac{m}{s}\right)$
Differential variables at t = 0	
$J_{w(0,y)}$ from: $J_{w(0,y)} = A_w\left((\Delta P_{b_{(0,y)}}) - RT_{b(0,y)}(C_{w(0,y)} - C_{p(0,y)})\right)$	
$J_{s(0,y)}$ from: $J_{s(0,y)} = B_s \cdot \exp\left(\frac{J_{w(0,y)}}{k_{(0,y)}}\right)(C_{b(0,y)} - C_{p(0,y)})$	
$C_{w(0,y)}$ from: $\frac{(C_{w(0,y)} - C_{p(0,y)})}{(C_{b(0,y)} - C_{p(0,y)})} = \exp\left(\frac{J_{w(0,y)}}{k_{(0,y)}}\right)$	
$C_{p(0,y)} = 0$	
Assigned variables at t = 0:	
$C_{b(0,y)}, F_{b(0,y)}, C_{p(0,y)}, F_{p(0,y)}, T_{b(0,y)}$ and $T_{p(0,y)}$ [These are same as $x = 0$]	

Table A.4. Grid sensitivity analysis

Operating conditions	Number of subdivisions	$C_{p(av)}$ x10^4 (kmol/m³)		$Rej_{(av)}$ (-)		$F_{b(outlet)}$ x10^4 (m³/s)	
		Exp.	Model	Exp.	Model	Exp.	Model
2.583x10^{-4} m³/s, 13.58 atm, 6.548x10^{-3} kmol/m³, 31.5 °C	4	2.296	1.740	97.3	98.019	2.011	1.935
	16	2.296	1.665	97.3	98.088	2.011	1.947
	36	2.296	1.796	97.3	97.921	2.011	1.952
	64	steep gradient problem of inefficient solution					

$2.166x10^{-4}$ m³/s, 11.64 atm, $4.092x10^{-3}$ kmol/m³, 31 °C	4	2.296	1.692	1.65	1.615	95.5	96.922
	16	2.296	1.620	1.65	1.626	95.5	97.025
	36	2.296	1.748	1.65	1.630	95.5	96.772
	64	steep gradient problem of inefficient solution					

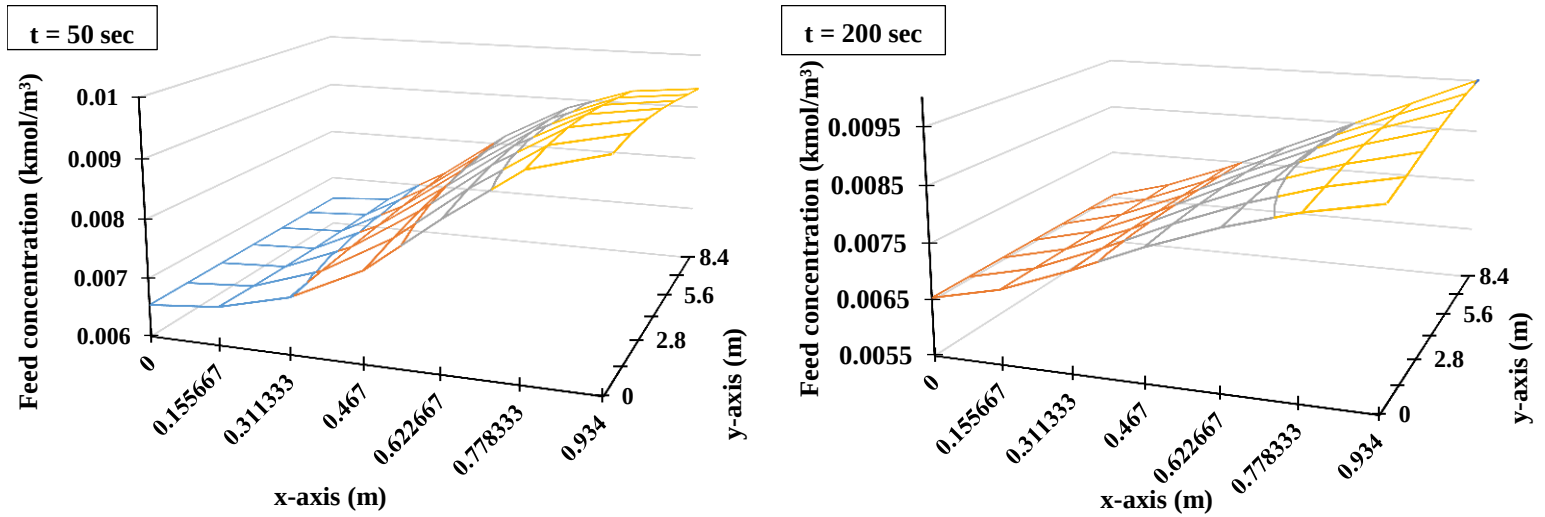

Fig. A1. Profile feed concentration along x-y axes of 36 sub-sections at two operating time (feed conditions: 2.166×10^{-4} m³/s, 6.548×10^{-3} kmol/m³, 13.58 atm and 31.5 °C)

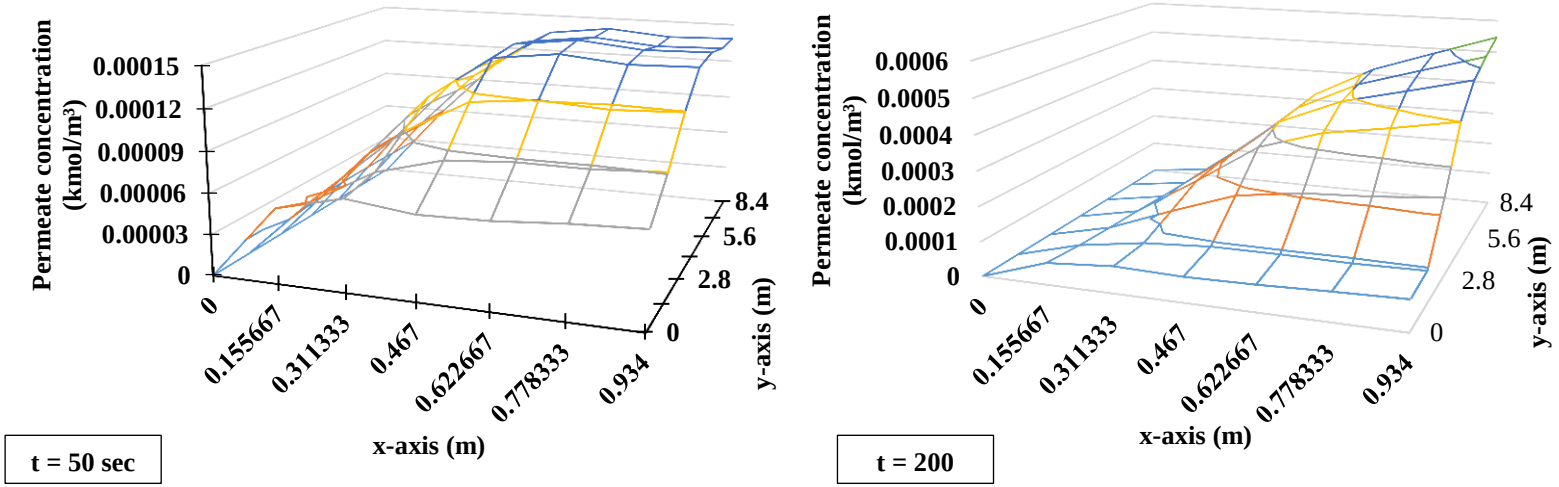

Fig. A2. Profile permeate concentration along x-y axes of 36 sub-sections at two operating time (feed conditions: 2.166×10^{-4} m³/s, 6.548×10^{-3} kmol/m³, 13.58 atm and 31.5 °C)

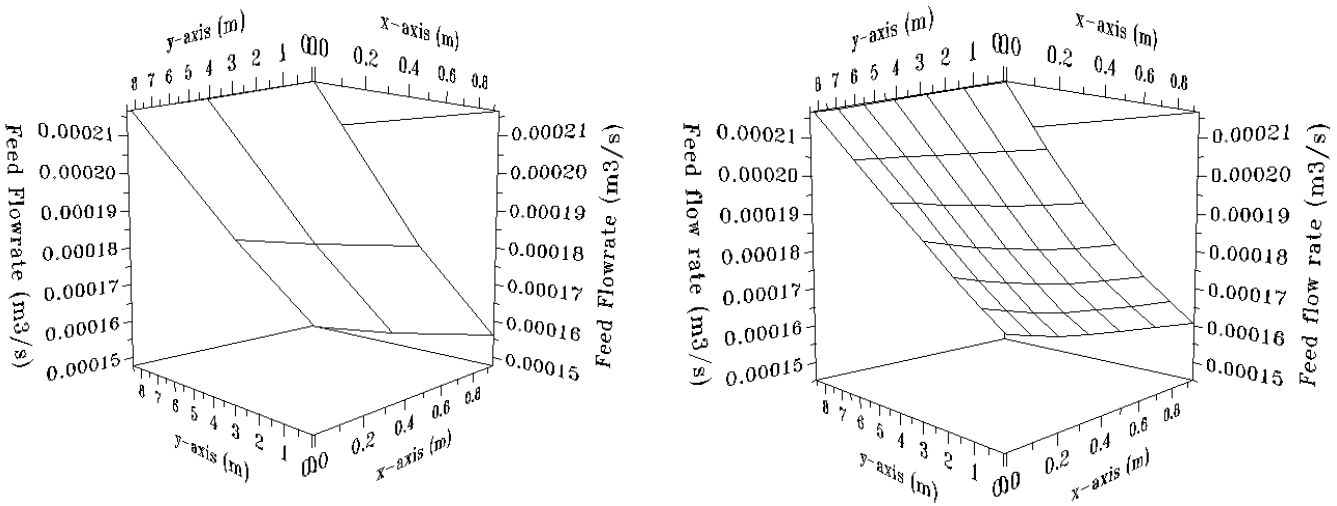

Fig. A3. Profile of Feed pressure along x-y axes of 4 and 36 sub-sections at t = 2000 sec (feed conditions: 2.166×10^{-4} m³/s, 6.548×10^{-3} kmol/m³, 13.58 atm and 31.5 °C)

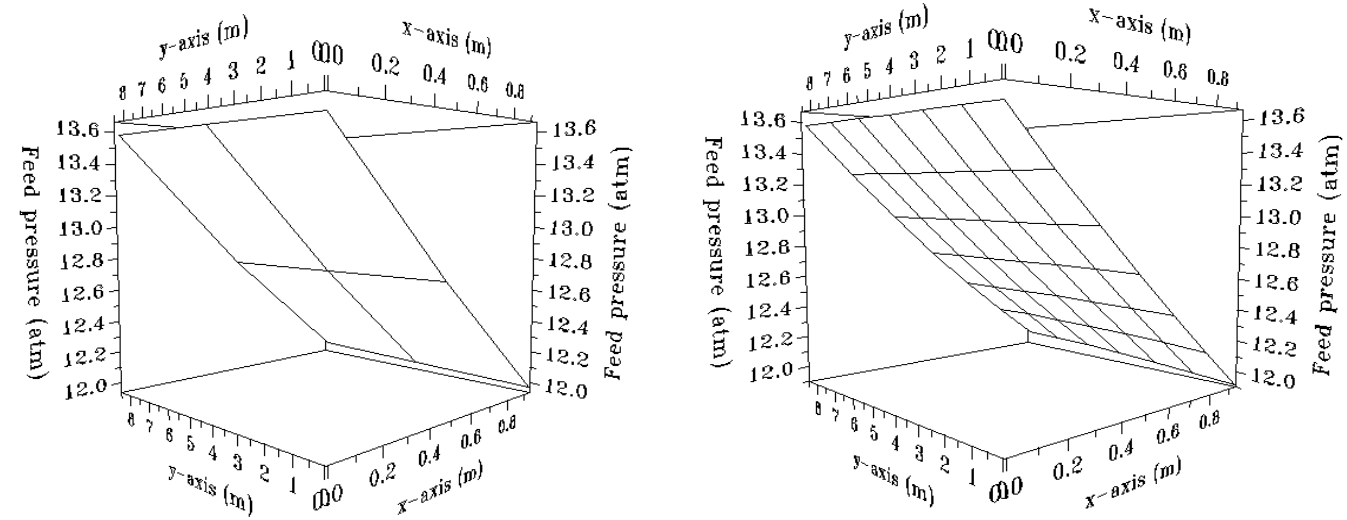

Fig. A4. Profile of feed flowrate along x-y axes of 4 and 36 sub-sections at t = 2000 sec (feed conditions: 2.166×10^{-4} m³/s, 6.548×10^{-3} kmol/m³, 13.58 atm and 31.5 °C)

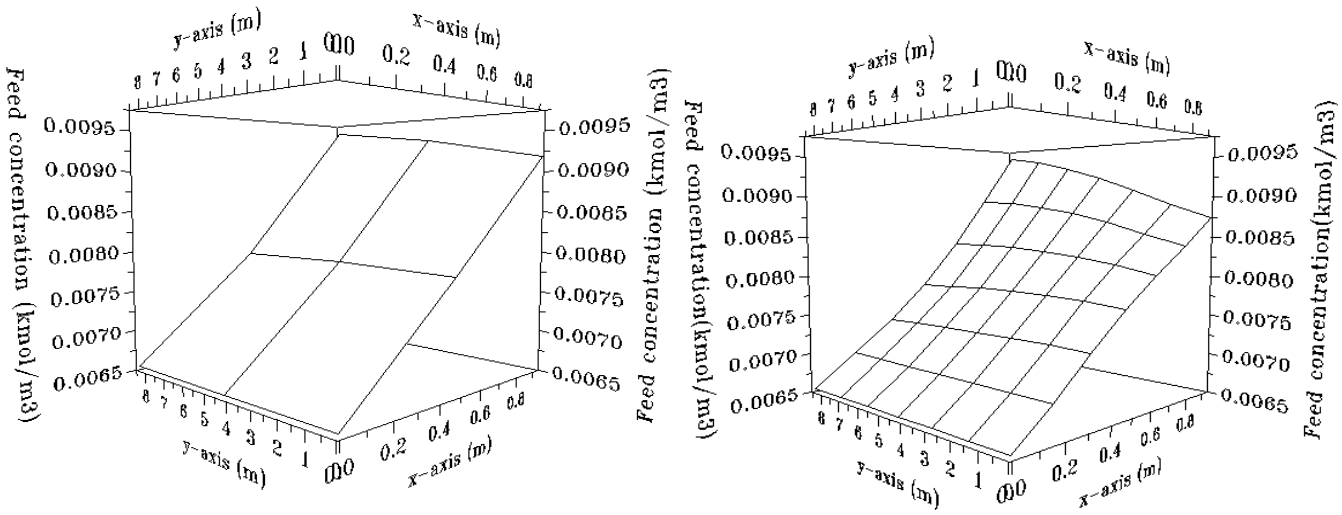

Fig. A5. Profile of feed concentration along x-y axes of 4 and 36 sub-sections at t = 2000 sec (feed conditions: 2.166×10^{-4} m³/s, 6.548×10^{-3} kmol/m³, 13.58 atm and 31.5 °C)

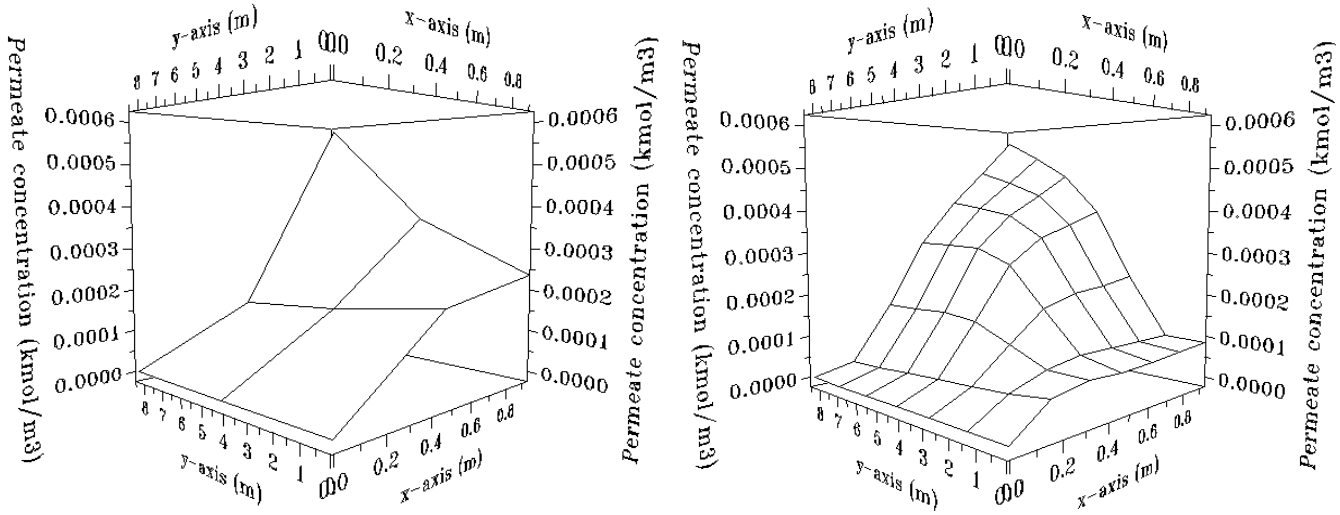

Fig. A6. Profile of permeate concentration along x-y axes of 4 and 36 sub-sections at t = 2000 sec (feed conditions: 2.166×10^{-4} m³/s, 6.548×10^{-3} kmol/m³, 13.58 atm, 31.5 °C)